Extraordinary Biomass-Burning Episode and Impact Winter Triggered by the Younger Dryas Cosmic Impact ~12,800 Years Ago. 2. Lake, Marine, and Terrestrial Sediments

31 authors, including:

Joanne P Ballard
U.S. Census Bureau
22 PUBLICATIONS **73** CITATIONS

SEE PROFILE

Andrew C Parnell
Maynooth University
120 PUBLICATIONS **6,648** CITATIONS

SEE PROFILE

Gabriela Domínguez-Vázquez
26 PUBLICATIONS **435** CITATIONS

SEE PROFILE

Some of the authors of this publication are also working on these related projects:

Project Coastal California Zooarchaeology View project

Project The Tell Tale Tusk View project

Extraordinary Biomass-Burning Episode and Impact Winter Triggered by the Younger Dryas Cosmic Impact ~12,800 Years Ago. 2. Lake, Marine, and Terrestrial Sediments

Wendy S. Wolbach,[1,*] Joanne P. Ballard,[2] Paul A. Mayewski,[3] Andrew C. Parnell,[4]
Niamh Cahill,[4] Victor Adedeji,[5] Ted E. Bunch,[6] Gabriela Domínguez-Vázquez,[7]
Jon M. Erlandson,[8] Richard B. Firestone,[9] Timothy A. French,[1] George Howard,[10]
Isabel Israde-Alcántara,[11] John R. Johnson,[12] David Kimbel,[13] Charles R. Kinzie,[1]
Andrei Kurbatov,[3] Gunther Kletetschka,[14] Malcolm A. LeCompte,[15]
William C. Mahaney,[16] Adrian L. Melott,[17] Siddhartha Mitra,[18]
Abigail Maiorana-Boutilier,[18] Christopher R. Moore,[19]
William M. Napier,[20] Jennifer Parlier,[21]
Kenneth B. Tankersley,[22] Brian C. Thomas,[23]
James H. Wittke,[6] Allen West,[21,†] and James P. Kennett[24]

ABSTRACT

Part 1 of this study investigated evidence of biomass burning in global ice records, and here we continue to test the hypothesis that an impact event at the Younger Dryas boundary (YDB) caused an anomalously intense episode of biomass burning at ~12.8 ka on a multicontinental scale (North and South America, Europe, and Asia). Quantitative analyses of charcoal and soot records from 152 lakes, marine cores, and terrestrial sequences reveal a major peak in biomass burning at the Younger Dryas (YD) onset that appears to be the highest during the latest Quaternary. For the Cretaceous-Tertiary boundary (K-Pg) impact event, concentrations of soot were previously utilized to estimate the global amount of biomass burned, and similar measurements suggest that wildfires at the YD onset rapidly consumed ~10 million km² of Earth's surface, or ~9% of Earth's biomass, considerably more than for the K-Pg impact. Bayesian analyses and age regressions demonstrate that ages for YDB peaks in charcoal and soot across four continents are synchronous with the ages of an abundance peak in platinum in the Greenland Ice Sheet Project 2 (GISP2) ice core and of the YDB impact event (12,835–12,735 cal BP). Thus, existing evidence indicates that the YDB impact event caused an anomalously large episode of biomass burning, resulting in extensive atmospheric soot/dust loading that triggered an "impact winter." This, in turn, triggered abrupt YD cooling and other climate changes, reinforced by climatic feedback mechanisms, including Arctic sea ice expansion, rerouting of North American continental runoff, and subsequent ocean circulation changes.

Online enhancements: appendix.

Introduction

In part 1 of this study (Wolbach et al. 2018, this issue), we investigated evidence of biomass burning at the Younger Dryas (YD) onset in six ice-core records on three continents. Here in part 2, we similarly compile and analyze data sets of biomass-burning proxies from 129 lake/marine records and

23 YD boundary (YDB) alluvial/colluvial sequences across four continents. The main purpose of both parts of this investigation is to examine the extent and magnitude of biomass burning at the YD onset and to determine its potential relationship to the YDB impact event. In addition, we explore whether these events initiated an "impact winter" that included YD climate change.

Firestone et al. (2007) posited that collisions between Earth and extraterrestrial objects occurred at the onset of the YD climate episode ~12,800 y ago, causing widespread catastrophic airbursts and/or

ground impacts. The YDB layer at more than 40 sites across North America, South America, Europe, and western Asia contains peak concentrations of one or more exotic YD-age impact-related proxies, including high-temperature iron-rich spherules, glassy silica-rich spherules, meltglass, platinum (Pt), iridium (Ir), and osmium (Os). Evidence for YDB biomass burning includes abundance peaks in carbon spherules, glass-like carbon, and nanodiamonds, with the focus of this study on charcoal and soot (aciniform carbon, denoted "AC/soot"; fig. 1). For images and detailed descriptions of proxies of biomass burning (wildfires), see figs. A1–A6; tables A1, A2; "Biomass-Burning Proxies Found at YDB Sites" in the appendix (the appendix, including figs. A1–A11 and tables A1–A13, is available online). Many publications that deal with the YDB impact event are provided in table A3.

To better understand potential YDB biomass burning, it is useful to investigate biomass burning caused by previously studied cosmic-impact events. One of those, the Tunguska airburst in 1908 over Siberia, created impact-related magnetic spherules, meltglass, nanodiamonds, and iridium, as discussed in Florenskiy (1965), Kirova and Zaslavskaya (1966), Firestone et al. (2007), Bunch et al. (2012), and Kinzie et al. (2014). This airburst produced a high-pressure blast wave energetic enough to topple 80 million trees across ~2000 km^2 (Florenskiy 1965; Svetsov 2008).

The thermal pulse scorched trees near the epicenter, before transient high temperatures rapidly subsided from >10,000°C at the center of the fireball. Numerous sampling sites at Tunguska indicate that temperatures and the severity of biomass burning decreased outward with distance from ground zero, initially igniting ~200 km^2 and subsequently spreading to consume ~500 km^2 of forest (Svetsov 2008). Because the impact-ignited fires were of low intensity, the burn layer contained charcoal amounts similar to those associated with normal, nonimpact ground fires (Svetsov 2008).

The most detailed study of impact-related biomass burning (Ebihara and Miura 1996) is of the 66-My-old Cretaceous-Tertiary boundary (K-Pg) event, which produced a discrete layer with peak abundances of numerous impact-related proxies, including extraterrestrial iridium and platinum (Arakawa et al. 2003). Although there is some debate about the magnitude of K-Pg biomass burning (Belcher et al. 2003; Robertson et al. 2013), the evidence includes concentration peaks in AC/soot (Wolbach 1990), charcoal (Robertson et al. 2013), carbon spherules (Adatte et al. 2005), annealed organic matter in framboidal pyrite (Mahaney 2002), and aerosol- and gas-phase polycyclic aromatic hydrocarbons (PAHs; Arinobu et al. 1999). The K-Pg impact event triggered wildfires that ranged widely in intensity from low-grade

Figure 1. Sites with Younger Dryas boundary (YDB) biomass-burning proxies. Circles represent 23 sites with wildfire proxies in the YDB layer, including charcoal and aciniform carbon/soot. See figure A7, available online, for locations of sites with YDB Pt peaks and figure A8, available online, for locations of lake and marine cores discussed in this investigation.

smoldering fires farther from ground zero, similar to natural wildfires, to high-intensity flaming combustion near ground zero that produced much less charcoal and more micron-sized carbon-rich aerosols and AC/soot (Wolbach 1990). The K-Pg AC/soot has been found globally at more than a dozen sites, and those concentrations were used to estimate the percentage of biomass burned as a result of the K-Pg impact event (Wolbach 1990; Wolbach et al. 1990, 2003). Atmospheric loading of AC/soot and other impact-related aerosols would have blocked nearly all sunlight from reaching Earth's surface, triggering extreme impact-related climate change by causing what is commonly referred to as an impact winter (Kaiho et al. 2016).

Increases in biomass burning related to YD climate change have been reported in eight independent studies that documented peak abundances of charcoal in lake cores and terrestrial sites ("Biomass-Burning Proxies Found at YDB Sites" in the appendix), and AC/soot at two sites in North America (Firestone et al. 2007). In addition, Maiorana-Boutilier et al. (2016) investigated organic-rich sedimentary layers called "black mats" at 19 sites in North America, Central America, Europe, and the Middle East and found peak abundances of black carbon/soot (BC/soot) and other biomass-burning proxies in the YDB layers. The full distribution of YDB AC/soot is unknown because few analyses have been conducted at sites on continents other than North America.

We investigated 152 terrestrial sites, marine cores, and lake cores on four continents to test the hypothesis that the anomalous peaks in YD biomass burning are coeval with the YDB impact event. The YDB layer offers an unprecedented opportunity to explore biomass burning associated with a major impact event that is young, well preserved, and relevant to human civilization.

Methods

Charcoal Record Selection. We compiled large data sets of biomass-burning proxies (e.g., charcoal and AC/soot) from 125 lake cores and 4 marine cores encompassing a wide range of environments: terrestrial, lacustrine, and marine. More than 8700 samples with depth and age values were available from across North, South, and Central America, Europe, and western Asia, the continents with known YDB impact evidence (figs. 1, A7, A8). For North America, 6046 samples were available, for Europe 676, for South America 1446, and for Asia 592; four were marine drilling sites. All of these sites were chosen because they are adequately dated, with calibrated

ages ≥10,000 cal BP and ≤15,000 cal BP, and also contain at least one sample dating between 13,400 and 12,300 cal BP. Most records are from the Global Charcoal Database (Power et al. 2008; GCD 2013). Sources and selection criteria for the data used in this study are given in "Sources of Data" and "Charcoal Record Selection" in the appendix.

Terrestrial Sites. Records from 23 YDB sites were chosen because they contained 453 adequately dated data points that span the YDB layer and include samples containing one or more biomass-burning proxies. These sites represent a wide range of geological settings, including coastal canyons, streambeds, caves, lakes, glacial moraines, and dune fields. Again, we limited data points to those with calibrated ages ≥10,000 cal BP and ≤15,000 cal BP that also contained at least one sample dating between 13,400 and 12,300 cal BP. Other YDB sites that contained impact-related proxies were not included because they are not adequately dated and/or have not yet been investigated for biomass-burning proxies (table A1).

AC/Soot. Fifteen sites were chosen for AC/soot testing where the YDB layer had been previously identified and dated. A standard protocol was used to extract AC/soot from bulk sediment (Wolbach et al. 1985, 1990; Wolbach and Anders 1989; Wolbach 1990; Kinzie et al. 2014). The process consists of multiple steps: (1) demineralization through multiple treatments of hydrofluoric acid (HF) and hydrochloric acid (HCl), (2) oxidation to separate organic material from elemental carbon by using sodium dichromate, (3) SEM analysis to differentiate between AC/soot and nonsoot carbon, and (4) examination of micrographs to quantify ratios of soot to nonsoot particle areas. For more details on quantifying AC/soot amounts, see "Extraction of AC/Soot from Sediments" in the appendix.

Platinum Measurements. Some Pt results are from previous studies. Eight new sites were chosen for this study where the YDB layer had been identified and dated and was known to contain impact-related proxies as well as biomass-burning proxies. Pt analyses were performed by Activation Laboratories, using fire assay and inductively coupled plasma mass spectrometry (ICP-MS; "Platinum Measurements" in the appendix) with standards and blanks to assure accuracy and replicability. Measurements are reported in parts per billion (ppb) dry weight, with a detection limit of 0.1 ppb.

Age-Depth Models. To create new age-depth models, we used Bayesian statistical analyses, which are able to calculate millions of possible age models (iterations) and determine the average (weighted mean; Bronk Ramsey 1998, 2009; Parnell et al. 2008;

Kennett et al. 2015). Because of this and other advantages, Bayesian age-depth modeling is considered more robust and flexible than non-Bayesian models (Parnell et al. 2008; Bronk Ramsey 2009), leading to the increased use of Bayesian analytical programs in multiple disciplines, for example, BChron (Parnell et al. 2008), BCal (Buck et al. 1999), OxCal (Bronk Ramsey 2009), and Bacon (Blaauw and Christen 2011). For this study, we used both BChron (ver. 3.2) and OxCal (ver. 4.2.4). We present all output by age at the 95% confidence interval (CI). For details, see "Age-Depth Models" in the appendix; an example of the OxCal code used is in "Example of Bayesian Age-Depth Code Used in OxCal" in the appendix.

Regression-Lowess Method. Once age-depths were calculated, we followed the regression-lowess protocol described by Power et al. (2008) and Marlon et al. (2009) as follows. Charcoal influx values were stabilized via the Box-Cox transformation and then converted to "Z-scores," which were calculated by subtracting the mean value and dividing by the standard deviation. Finally, Z-score values were smoothed with a lowess algorithm, typically with ~200-y half-windows. For details, see "Regression-Lowess Method" in the appendix

Bayesian Errors-in-Variables (EIV)-Spline Method. Radiocarbon dates were calibrated with IntCal13 within the OxCal program (ver. 4.2.4; Bronk Ramsey 1998, 2009) to produce Bayesian age-depth models. Charcoal influx values were then converted to Z-scores, as described in the regression-lowess method. A Bayesian EIV algorithm, developed by Cahill et al. (2015), was used to plot the Z-scores. The algorithm was designed to run within the Bayesian program BChron (Haslett and Parnell 2008; Parnell et al. 2008), and within the open-source statistical software program R. For details, see "Bayesian EIV-Spline Method" in the appendix. The BChron and EIV programming code used here can be obtained from coauthor A. C. Parnell at https://maths.ucd.ie /~parnell_a/.

Results

Utilizing YDB Platinum (Pt) as a Datum. Petaev et al. (2013b) examined samples from the Greenland Ice Sheet Project 2 (GISP2) ice core and identified a large Pt spike, which they attributed to an extraterrestrial-impact event at the YD onset. These workers inferred "multiple injections of Pt-rich dust into the stratosphere that are expected to result in a global Pt anomaly" (p. 12,917). Their results indicate that extraterrestrial Pt settled out of the atmosphere into a 21-y interval of ice, rising 100 times above background at 12,822 ± 140 cal BP, within the range

12,836–12,815 cal BP. Including this discovery, there have been multiple independent reports of Pt abundance peaks in the YDB layer at 22 sites in North America, Europe, and Asia: one site in Greenland (Petaev et al. 2013b), one site in Russia (Andronikov et al. 2014), four sites in Lithuania (Andronikov et al. 2015), one site on the French-Italian border (Mahaney et al. 2016b), two sites in the Netherlands (Andronikov et al. 2016b), one site in Belgium (Andronikov et al. 2016b), and 12 sites in the United States (Andronikov and Andronikova 2016; Moore et al. 2017).

Quantifying YDB Pt Concentrations. In this study, peaks in YDB Pt abundances were identified at 8 out of 10 sites (fig. 2; table A6). For two sites, Pt has not yet been measured, so instead, abundances are shown for magnetic impact-related spherules. Six sites show high, distinct YDB peaks in Pt abundances, and two had smaller peaks. In all, 71 samples were analyzed, and of those, 51 were identified as having background values that averaged 0.2 ppm (range: <0.1–0.5), and 20 were considered to be YDB impact values, averaging 1.4 ppb, or 7 times the background value (range: 0.5–8.1). Thus, YDB peaks in Pt were observed at 28 sites, including those of this study and previous studies. For previously published studies of key YDB sites, see table A1.

Analyzing YDB Biomass-Burning Proxies at Terrestrial Sites. Biomass burning produces a wide variety of carbon-rich proxies, including charcoal, soot, carbon spherules, and glass-like carbon. Although nanodiamonds have never been found associated with nonimpact wildfires, they often are found in YDB carbon spherules and glass-like carbon (Kinzie et al. 2014), and therefore we consider them to be an indirect proxy for impact-related wildfires.

One particularly important biomass-burning proxy is AC/soot, a subset of the BC/soot group. Scanning electron microscopy reveals that AC/soot has a clearly distinguishable morphology resembling bunches of grapes, the definition of "aciniform." Particles of AC/soot with diameters typically <1 μm are readily distributed throughout the atmosphere during wildfires, as exhibited by the 66-My-old K-Pg impact that distributed them across multiple continents (Wolbach 1990).

Firestone et al. (2007) observed AC/soot abundance peaks at two sites in Arizona and South Carolina. Both occurred in the YDB and adjacent layers, with no AC/soot above or below. Later, Maiorana-Boutilier et al. (2016) measured BC/soot at 19 YDB sites: nine in the United States, seven in Mexico, and one each in Belgium, Syria, and Spain. They examined 34 terrestrial YDB samples of dark, organic-rich sedimentary layers, known as "black
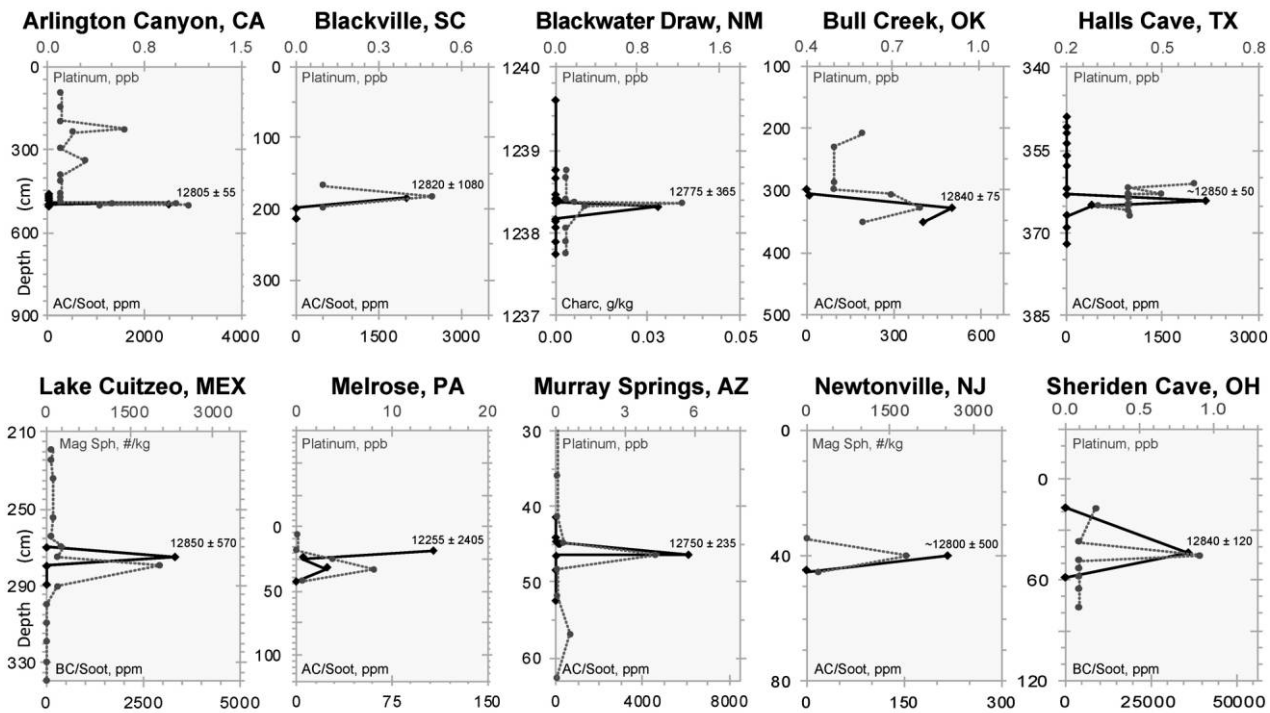
Figure 2. Younger Dryas boundary (YDB) biomass-burning proxies plotted against impact-related proxies from 10 selected terrestrial sites. Black solid lines represent either Pt (ppb) or magnetic spherules ("Mag Sph, #/kg"); dotted gray lines represent aciniform carbon (AC/soot; ppm), black carbon (BC)/soot (ppm), or charcoal (Charc.; g/kg). Bayesian-calculated ages on the right-hand side are from Kennett et al. (2015).

mats" (Haynes 2008). Measurements were made on these samples for stable carbon isotopic ratios ($\delta^{13}C_{soot}$), abundances of BC/soot (a larger group that includes AC/soot), and levoglucosan (a marker for biomass combustion). All sites contained peak concentrations of BC/soot in the YDB layer. Concentrations of levoglucosan from within the black-mat layer in Ohio were ~125 times higher than those in the layer below it, signaling a significant peak in biomass burning. Even though the sampling sites extended across two continents, $\delta^{13}C_{soot}$ values from the YDB black mats were similar across all sites and yet different from the $\delta^{13}C_{soot}$ values measured above and below the YDB layer. These results suggest that the fuel sources of YDB biomass burning were ex situ and mixed, supporting the hypothesis of intense, widespread, coeval wildfires across North America and Europe.

In this study of AC/soot, all selected sites included a dated YDB layer with at least one proxy for biomass burning. Analyses were performed on samples from 16 terrestrial sites in five countries: 12 sites in 10 US states and one site each in Belgium, Canada, Mexico, and Syria. The sites are located up to ~12,000 km apart, and their records contain an av-

erage of three impact-related wildfire proxies each (range: 1–7). The settings of sites are highly variable, including a coastal canyon (Arlington Canyon, Santa Rosa Island, CA), a Carolina bay (Blackville, SC), seasonal, arid-region streambeds (Blackwater Draw, NM; Bull Creek, OK; Murray Springs, AZ), caves (Hall's Cave, TX; Sheriden Cave, OH), a fresh-water lake (Lake Cuitzeo, Mexico), an end-glacial Moraine (Melrose, PA), and a relict dune field (Newtonville, NJ).

Quantifying YDB AC/Soot. Of the 15 terrestrial sites, seven contain detectable YDB AC/soot. Two sites previously investigated by Maiorana-Boutilier et al. (2016) contained BC/soot, but in this study, only one of those sites contains detectable AC/soot (fig. 1; tables A4–A6). For nine of the 10 sites shown in figure 2, there were measurable YDB biomass-burning peaks in either AC/soot or BC/soot. The tenth site (Blackwater Draw, NM) contains no measurable AC/soot, and so abundances are shown for charcoal. We analyzed 78 sediment samples from the 15 sites and determined an average value of 1234 ppm, with a range from 100 to 6100 ppm (0.6 wt% of bulk sediment). On the basis of SEM imaging, the AC/soot particles range in size from ~10 to 150 nm. The YDB

AC/soot is indistinguishable from K-Pg AC/soot in size and shape, and the size ranges of AC/soot for both impact events have lognormal distributions (Wolbach et al. 1985; Wolbach and Anders 1989). Concentrations of AC/soot were found only in and/or contiguous to the YDB layer, with none detectable in 51 sedimentary samples above and below the YDB. Charcoal produced by nonimpact wildfires and anthropogenic campfires occurs above and below the YDB at many of the 15 sites, and yet no AC/soot was detected, consistent with the interpretation that AC/soot from nonimpact wildfires is rarely preserved (Wolbach et al. 1985; Wolbach and Anders 1989; Wolbach 1990),

Quantifying Charcoal at Terrestrial YDB Sites. Sedimentary charcoal was identified via optical microscopy in 287 sediment samples. We detected YDB peak charcoal concentrations at 31 sites, ranging in diameter from ~125 μm to 6 cm and in abundance at the YDB from a few dozen particles to 27.9 g/kg, averaging 3.9 g/kg (fig. 2; table A6). Background concentrations average 0.1 g/kg, with a range of 0–1.5 g/kg. Peak abundances of charcoal in the YDB layer always co-occur with one or more peaks in AC/soot, carbon spherules, glass-like carbon, nanodiamonds, high-temperature meltglass, impact-related microspherules, Ir, or Os.

Analyzing YDB Biomass-Burning Evidence in Lake and Marine Cores. The YDB hypothesis predicts that many, but not necessarily all, lake-core records should contain evidence of significant peaks in biomass burning at the YD onset, and there are many examples of such peaks in the existing literature. (1) In the northeastern United States, Munoz et al. (2010) examined 40 charcoal records and found an above-background collective charcoal peak that dates to the YD onset. (2) Similarly, in Europe, Kaiser et al. (2009) sampled across the YD-age Usselo Horizon at 29 sites across 600 km of northern Europe (Belgium, the Netherlands, Germany, and Poland). At approximately half the sites, they found "conspicuous amounts of . . . charcoal" (p. 601) near or in the YDB layer, some of which they noted were associated with possible impact proxies. (3) In Scotland, Edwards et al. (2000) conducted high-resolution pollen and microscopic charcoal analyses in numerous late Quaternary paleolake and wetland sequences. They documented an anomalous sharp rise in charcoal content at or close to the onset of YD cooling (locally called the "Loch Lomond Stadial") that rose to a distinct abundance peak during the YD episode. The authors expressed difficulty in explaining the origin of the anomalous burning episode because of low biomass availability in Scotland at that time, suggesting that the charcoal may have had

a nonlocal source. (4) Power et al. (2008; their fig. 5) conducted a low-resolution study of 355 charcoal records from the Global Charcoal Database (GCD) for North America, Europe, and Africa and found a peak in YD-age charcoal in the 500-y bin 13,000–12,500 cal BP. (5) Daniau et al. (2010) produced low-resolution 400-y bins of charcoal concentrations for 67 sites in Africa, Asia, Australia, Europe, North America, and South America (their fig. 4). They identified a major collective charcoal peak during the YD climate episode, representing one of the highest charcoal abundance peaks in the previous 25,000 y.

Quantitative charcoal records are commonly produced during paleoecological investigations of lake sediment cores that have been radiocarbon dated, and these data are readily available from international data repositories. Mostly using the GCD (2013), we compiled and analyzed charcoal records from multiple lake cores on four continents. This investigation was restricted to the interval between ~14,000 and 12,000 y ago, a span that includes the YDB impact event at 12,835–12,735 cal BP (Kennett et al. 2015).

Central to this study is the requirement of uniformly calibrated radiocarbon dates for use in developing accurate age-depth models and for intercore correlations. Related to this, we address several problems that are common to comparative studies of lake-core charcoal records. First, it has long been common practice to compile and compare lake records in which ^{14}C dates had been calibrated with different radiocarbon calibration curves (e.g., IntCal93, IntCal98, IntCal04, IntCal13, and Fairbanks 0805). However, these curves are mutually incompatible, potentially resulting in large differences between them for an identical radiocarbon date. For example, calibration of the ^{14}C date of 10,900 $\pm$ 100 [14]C y BP (12,819 $\pm$ 94 cal BP; IntCal13) using these five different radiocarbon curves produces calibrated ages that vary by up to 117 y (table A7). Such high variability for calibrations of the same radiocarbon date seriously decreases the accuracy of intercore comparisons.

We also reexamined 35 dated lake-core records investigated by Marlon et al. (2009) and calibrated the single radiocarbon date nearest the YD onset, using four different calibration curves (IntCal93, IntCal98, IntCal04, and IntCal13). Our results show a substantial age difference of more than 1000 y (from +520 to −533 y; table A8). The average chronological resolution (age uncertainty) with the latest calibration curve, IntCal13, for the same 35 North American lake-charcoal records is $\pm$179 y, rather than $\pm$50 y, as claimed by Marlon et al. (2009; fig. A9; table A9). Therefore, dates for all records used
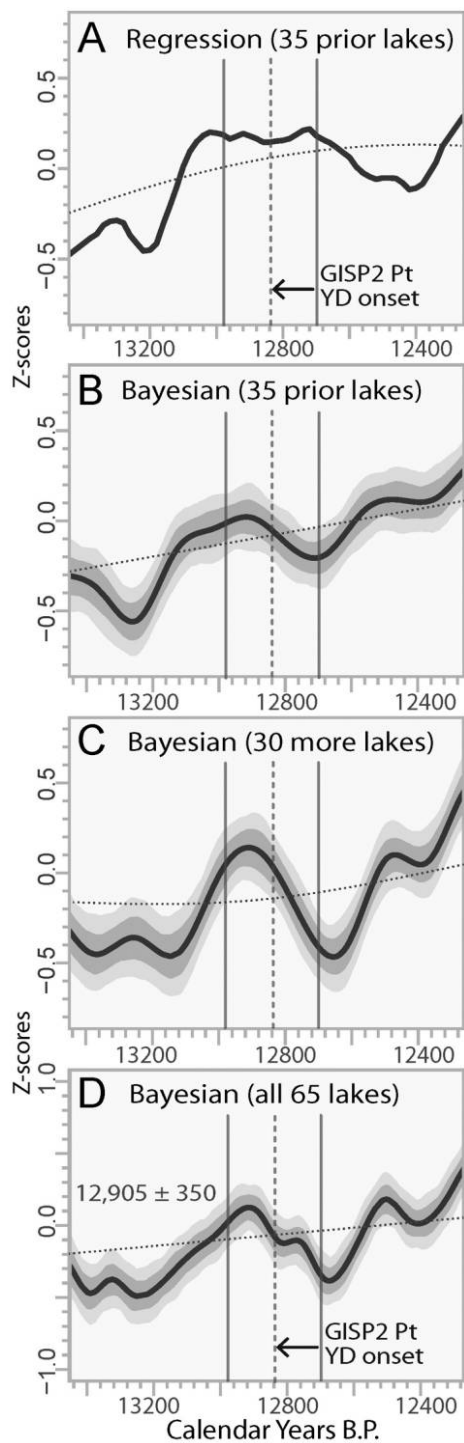
Figure 3. Comparison of regression-lowess and Bayesian EIV (errors-in-variables)-spline models for charcoal concentrations in 65 North American lakes. The Y-axis plots Z-scores of charcoal concentrations. Black lines represent mean ages; dark gray curved bands represent Z-scores at the 68% confidence interval (CI) and light gray bands that at the 95% CI. The vertical dashed line represents the age of the Pt spike in the Greenland Ice Sheet Project 2 (GISP2) core, and the vertical solid lines repre-

in this study were recalibrated with a single current calibration curve, IntCal13 (Reimer et al. 2013).

It has also been common practice to create age-depth models by using regression algorithms that produce single point dates (calibrated median or mean ages) that lack age uncertainties. This incorrectly assumes that lake charcoal dating to, for example, 12,800 cal BP is accurate to within ± 0 y, an unsupportable level of precision (see Kennett et al. 2015). Recognizing this limitation, curators of the Neotoma Database for charcoal data recommended that age-depth models provided to international databases include calibrated age uncertainties.

The chronological resolution of the lake records used in this study ranges from high to low quality. The issue of low-resolution sampling was considered by Marlon et al. (2009), who found that including some low-resolution records had little or no effect on the results for the 35 lakes in their study (see their fig. 1). Similarly, Kennett at al. (2015) found little or no difference caused by mixing low-resolution records with high-resolution ones (see their figs. 9 and S22). For our study, low-resolution sampling is mitigated by the use of Bayesian analysis, in which high-resolution dates are weighted more to compensate for the low-resolution records.

In this study, we analyzed charcoal records from 125 lakes and four marine cores on four continents (table A10), using one of two methods for comparison: (1) the regression-lowess method (without age uncertainties) and (2) the Bayesian EIV method (with age uncertainties), as described in "Methods."

Analyzing Lake and Marine Charcoal Concentrations. North American Lake Records of Biomass Burning. First, we used the same regression-lowess method for the 35 lakes reported by Marlon et al. (2009; their fig. 2) and produced identical results (fig. 3A). The resulting curve demonstrates a sharp rise in charcoal at ~13,040 cal BP, near the YD onset, that Marlon et al. (2009, p. 2522) reported to be "the largest and most rapid change in biomass

sent the GISP2 timescale uncertainties of ± 140 y (Greenland Ice Core Chronology 2005 timescale [b2k]; Rasmussen et al. 2008; Seierstad et al. 2014). Roughly horizontal dotted lines represent sixth-order polynomial trend lines. The vertical dashed line indicates Pt enrichment and Younger Dryas (YD) cooling onset in the GISP2 ice core (Petaev et al. 2013b). A, Lowess-smoothed model of 35 lakes from the Global Charcoal Database, as presented by Marlon et al. (2009). B, Bayesian model using identical data from the same 35 lakes. C, Bayesian age-depth model for 30 additional North American lakes. D, Bayesian age-depth model for all 65 North American lakes, with YD boundary peak at 12,905 $\pm$ 350 cal BP.

burning during deglaciation. Burning was widespread but not continent wide." There are oscillations around a general trend of gradually increasing wildfire activity during the deglacial period from ~13,400 to 12,300 cal BP, and all peaks above the trend lines in figure 3 are standard deviations representing significant episodes of biomass burning.

Bayesian analysis of the same 35 lake-charcoal profiles produced a curve that is generally similar to the regression-lowess model (fig. 3A), but with important differences. There is a broad-based peak dated to 12,905 ± 485 cal BP that overlaps the previously published YDB age of 12,835–12,735 cal BP at 95% CI (Kennett et al. 2015). The Bayesian analytical plot (fig. 3B) places the charcoal peak ~100 y younger than the regression-lowess plot (fig. 3A), even though they use the same data set. This difference most likely results from calibrating the dates with a single calibration curve instead of multiple ones and from using Bayesian instead of regression analyses. Bayesian modeling is generally considered more robust, because it provides statistical uncertainties for both Z-scores and ages, rather than erroneously assuming that the statistical accuracy is ±0 y.

We also analyzed 30 additional lake records in the United States (18 states) and Canada (five provinces) compiled from the GCD (2013) and independent papers. The samples range in age from 13,400 to 12,300 cal BP, a span selected to include the YD onset. The results show a pronounced YDB charcoal peak at 12,900 ± 280 cal BP (fig. 3C), similar to that of the 35 lakes previously analyzed (fig. 3B).

We combined data for the 35 lakes from Marlon et al. (2009) with the 30 additional records, for a total of 65 lake records. The records contain 6046 dates, for an average of 93 dated charcoal records per lake with an average chronological sample resolution of ~40 y. Charcoal plots for eight North American lakes selected from the group are shown in figure A10. Charcoal and soot records are shown for one North American lake in figure A11. As calculated by the EIV routine, there are several above-mean charcoal peaks in the record, and one of the highest occurred at 12,905 ± 350 cal BP (13,255–12,555 cal BP) at 95% CI, overlapping the age of 12,835–12,735 cal BP for the YDB event (Kennett et al. 2015).

Charcoal Z-score peaks across four continents display an observable pattern (fig. 4), in which the collective YD-age charcoal peak, labeled "3," falls within an approximately 100-y span for values on all continents. The age of each peak 3 is shown at the bottom right of each panel. The pattern of several peaks for North America (fig. 4A) closely corresponds to that for Europe (fig. 4C), but other than the peak at the YD onset, South/Central America (fig. 4E) and Asia (fig. 4G) showed little similarity to each other or to North America and Europe. Thus, wildfire activity at the YD onset appears to be coeval on all continents, suggesting a panhemispheric external forcing mechanism, such as the YDB impact event and ensuing YD climate change. Wildfire activity at other times is not coeval across continents, thus making synchronous biomass burning unique to the YD onset.

European Lake Records of Biomass Burning. For nine European countries, we analyzed charcoal records from 19 lake cores. There are 676 samples with interpolated dates, for an average of 36 dated charcoal records per lake with an average chronological resolution per sample of ~90 y. The EIV results (fig. 4C) show an increase in wildfire activity near the YD boundary, rising to a mean peak at 12,835 ± 220 cal BP (13,065–12,625 cal BP), overlapping the Bayesian-calculated YDB age range of 12,835–12,735 cal BP (Kennett et al. 2015). Regression-lowess results for Europe show a similar trend (fig. 4D).

South and Central American Lake Records of Biomass Burning. For nine countries, we analyzed 28 lake sediment records containing 1446 interpolated ages, for an average of 52 dated charcoal records per lake with an average sample span of ~85 y. One of the highest peaks in the record occurs at the YD onset, 12,850 ± 235 cal BP (fig. 4E; 13,085–12,545 cal BP). Regression-lowess results are similar (fig. 4F).

Asian Lake Records of Biomass Burning. In seven countries across Asia, we investigated 17 sites containing 592 dates, for an average of 35 dated charcoal records per lake. The average sample span is ~120 y. There is a conspicuous peak in mean charcoal abundances at 12,950 ± 225 cal BP (13,175–12,725 cal BP), followed by a sharp decline in biomass burning and then a peak at 12,400 cal BP (fig. 4G). Regression-lowess results are similar (fig. 4H).

Marine Records of Biomass Burning. We examined the Global Charcoal Database to identify marine records that met the criteria of this study. This revealed only four cores with charcoal and/or soot abundances that were adequately dated at sufficient resolution. Two cores, MD95-2042 near the coast of Spain and 17940 from the South China Sea, show multiple charcoal peaks, including ones at or close to the YDB, but these peaks are unremarkable, perhaps because of the low resolution of the cores. Each record was statistically grouped and analyzed with the terrestrial lake records of the nearest continent.

One well-dated, high-resolution late Pleistocene core (Ocean Drilling Program Hole 893A) is from the Santa Barbara Basin off the coast of California.
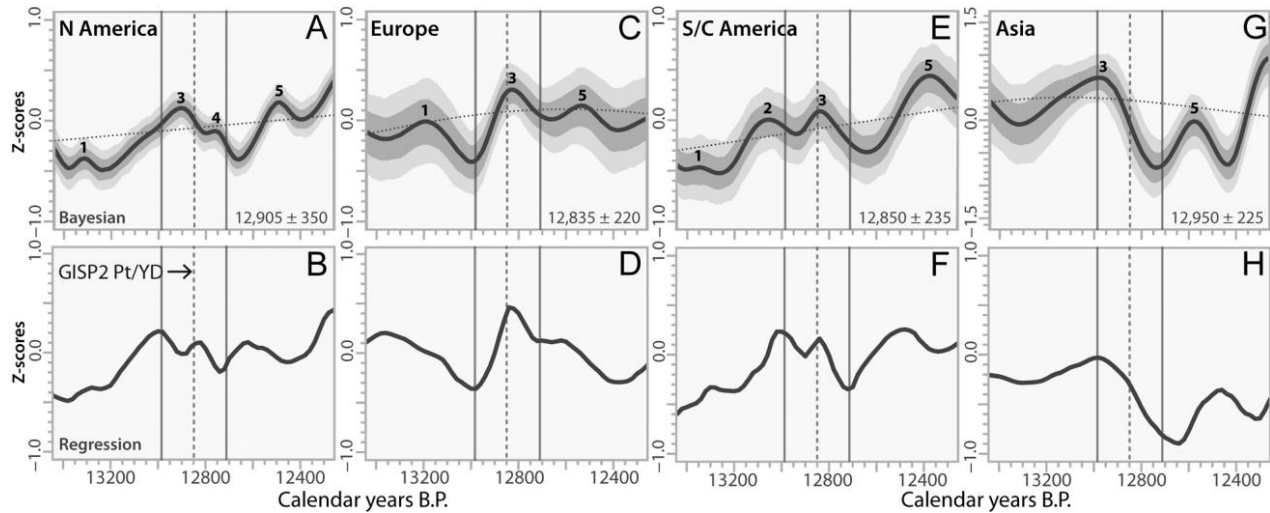
Figure 4. Comparison of Bayesian EIV (errors-in-variables)-spline models for 129 charcoal records from five continents: Z-scores versus age. Solid black lines represent mean ages calculated by the EIV method; dark gray bands represent Z-scores at the 68% confidence interval (CI) and light gray bands those at the 95% CI. Dashed vertical lines indicate Greenland Ice Sheet Project 2 (GISP2) Pt peak median age, and solid vertical lines represent ice-core age uncertainties of ±140 y (Greenland Ice Core Chronology 2005 timescale). Roughly horizontal dotted lines represent sixth-order polynomial trend lines; highest peaks are above mean. Peak values in each curve are labeled 1–5; not all peaks appear in each plot. Ages shown in lower right-hand corners (*A, C, E, G*) are for values at peak 3 (across the Younger Dryas [YD] onset); ages for all peak 3s fall within a span of ~100 y. *A*, Bayesian EIV-spline model for 65 North American lakes, as in figure 3*D*. *B*, Regression-lowess model for same data. *C, D*, Bayesian EIV-spline (*C*) and regression-lowess (*D*) models for 19 European lakes. *E, F*, Bayesian EIV-spline (*E*) and regression-lowess (*F*) models for 28 South/Central (S/C) American lakes. *G, H*, Bayesian EIV-spline (*G*) and regression-lowess (*H*) models for 17 Asian lakes. Bayesian EIV-spline and regression-lowess models are similar to the lowess curves, except that the corresponding charcoal peaks are somewhat older or younger and curve amplitudes differ.

This 24,000-y sequence exhibits the highest peak in biomass burning precisely at the YD onset, on the basis of the charcoal-pollen ratio (Heusser and Sirocko 1997). This anomalously high peak correlates with intense biomass burning documented from the nearby Channel Islands (Kennett et al. 2008). The peak also coincides with the extinction of pygmy mammoths on the islands and with the beginning of an apparent 600–800-y gap in the archaeological record, suggesting a sudden collapse in island human populations (Kennett et al. 2008).

Another valuable marine core record of biomass burning is from the western Pacific >500 km north of Papua New Guinea (MD97-2140, water depth 2547 m; Thevenon et al. 2004). This core is unusual in providing a record not only of charcoal but also of black carbon, which includes AC/soot. The record exhibits two high black-carbon peaks in the ~368,000-y-long biomass-burning record, the first at ~50,000 y ago and the second spanning the age interval from 13,291 to 12,515 $\pm$ 125 cal BP (fig. 5) and overlapping the YD onset at ~12,800 cal BP. In addition, the YDB peak in black carbon coincides

with an above-average charcoal peak at ~12,750 cal BP (Thevenon et al. 2004). The coincidence of these peaks at the YD onset with similar peaks on four continents suggests a connection to the YDB impact event, rather than to anthropogenic burning, as suggested by Thevenon et al. (2004).

YDB Wildfire Magnitudes. The magnitude of a stratigraphic charcoal peak is not necessarily proportional to wildfire intensity or the land area burned (Marlon et al. 2009). Even so, previous studies show that unusually high charcoal peaks in the historical record have been linked to intense, large-scale fires (Marlon et al. 2009; Clark and Patterson 1997; Clark et al. 1998; Lynch et al. 2004). To assist in evaluating the relative magnitude of wildfire episodes at or near the YD onset, we identified the age of the highest and second-highest charcoal concentration peaks in each of the same group of 129 charcoal lake/marine records dating to between 15,000 and 12,200 cal BP, a span of 2800 y. This age interval was marked by two major episodes of rapid climate change: the cold-to-warm transition at the onset of the Bølling (~14,400 cal BP) and the warm-to-cold transition at the onset of the
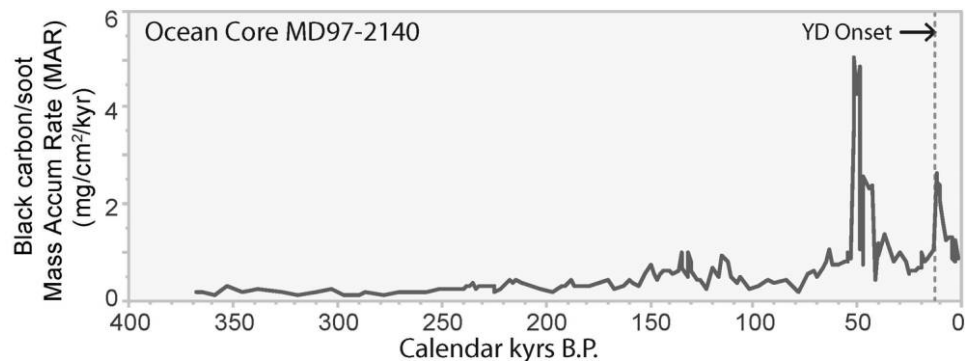
Figure 5. Black carbon/soot in a western Pacific Ocean core, Papua New Guinea. Two major peaks are shown. The second-highest black carbon/soot peak spans the Younger Dryas boundary (YDB) interval, rising to ~4 times the background level. The Y-axis shows accumulation rate (Thevenon et al. 2004). Vertical dashed line represents the Younger Dryas (YD) onset and the YDB Pt peak.

YD (~12,800 cal BP). Charcoal peaks were identified according to the protocol described by Marlon et al. (2009). We grouped these ages into 400-y bins, which, at ±200 y, is similar to the average age uncertainty (±179 y) for 35 North American lake-charcoal records. Of the 129 lake records, 118 exhibited charcoal peaks between 15,000 and 12,200 cal BP. The remaining 11 lake records were discontinuously sampled at low resolution, providing few data points.

For all continents investigated—North America, Europe, Asia, and South America—the highest binned peaks span the onset age of the YD climate episode from 13,000 to 12,600 cal BP. The individual continents show similar results: 44%–30% of the highest charcoal peaks for each continent fall within the same bin that includes the YD onset and the GISP2 Pt peak (fig. 6). This represents an anomalously large cluster of wildfires, unequaled by fire activity for the other intervals.

For the binned results on all four continents, ~33% of the highest peaks in the 118 records fall within the bin centered at 12,800 ± 200 cal BP (fig. 7A). For the four continents, 66% of lakes (85 of 129) contain one or more charcoal peaks from wildfires within the range of 12,800 ± 150 cal BP (fig. 7B), closely matching the age of the Pt peak at 12,822 ± 140 cal BP. Another 17% of lake records (22 of 129) showed at least one charcoal peak from a wildfire in the range of 12,800 ± 300 cal BP. The remaining 17% of lakes (22 of 129) that exhibited no significant charcoal peaks in that interval were discontinuously sampled at low resolution, with only a few samples in the entire 2800-y interval.

Bayesian Analysis of Synchroneity at the YD Onset. The YDB hypothesis predicts synchroneity at the YD onset among multiple proxies, including YDB cosmic-impact proxies and biomass-burning proxies

in ice cores, terrestrial sites, lake cores, and marine cores. Radiocarbon age uncertainties are too large to permit conclusive proof of synchroneity at the YD onset. Therefore, we used Bayesian analysis to determine whether synchroneity is statistically possible, following Parnell et al. (2008) and Bronk Ramsey (2009) in using OxCal's Bayesian difference code. If the Bayesian-calculated intervals at the 68% and 95% CIs allow for a full overlap of all records (i.e., include 0 y as a possibility; reported in OxCal as −1), then the ages of all the YDB events could be statistically synchronous. On the other hand, if the CIs include only values that are greater than 0, synchroneity is rejected.

Bayesian analysis shows that the mean age is 12,854 ± 56 cal BP (12,910–12,798 cal BP), which overlaps the Bayesian-calculated age of 12,835–12,735 cal BP (fig. 8; table A11; Kennett et al. 2015). OxCal also computed age intervals of −1 to 268 y at the 68.2% CI, −1 to 655 y at the 95.4% CI, and −1 to 1291 y at the 99.7% CI. All three CIs contain 0, meaning that they could overlap in age, and there are no grounds to reject synchroneity, thus supporting YDB impact theory.

Discussion

Evidence from widely separated ice records in part 1 (Wolbach et al. 2018) and sediment records here in part 2 demonstrates that a major, widespread peak in biomass burning occurred on at least four continents at the warm-to-cold transition marking the YD onset (fig. 9A, 9B). This peak is synchronous with the YDB cosmic-impact layer, as recorded by multiple impact-related proxies, including peak abundances of Pt, high-temperature microspherules, and meltglass.
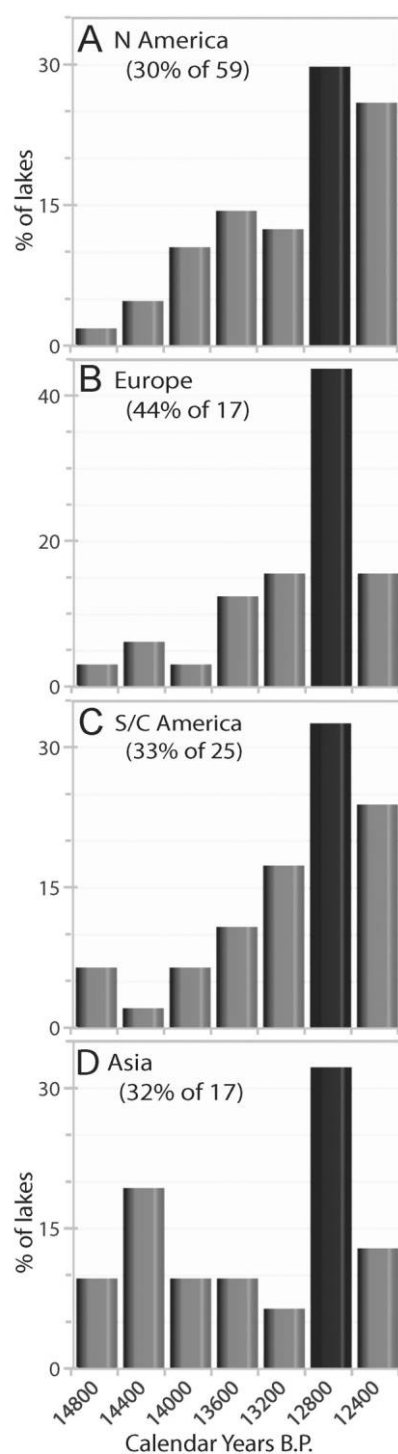
Figure 6. Fire frequency on four continents: seven 400-y bins across a 2800-y interval (15,000–12,200 cal BP) that includes the Younger Dryas onset. Bars represent the sum of the numbers of highest and second-highest peaks for 118 lake records combined into 400-y bins. Younger Dryas boundary bin range = 44%–30%. S/C America = South/Central America.
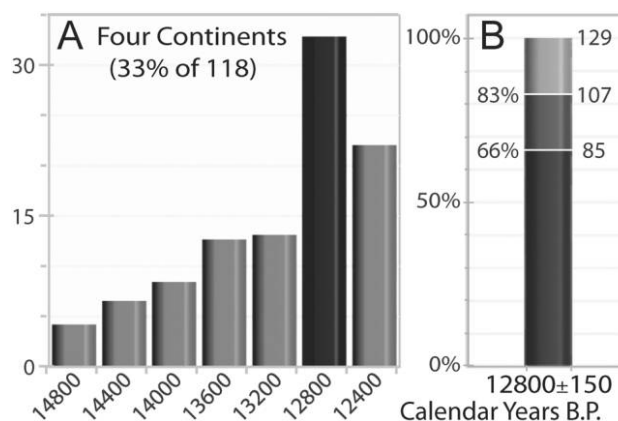

Figure 7. Fire frequency totals. *A*, Bars represent the sum of the numbers of highest and second-highest peaks for 118 lakes compiled in seven 400-y bins spanning 15–12.2 ka. The bin centered on 12,800 cal BP contains 33% of the total peaks, ~4 times the average of all other peaks. *B*, Cumulative total of individual biomass-burning peaks: 66% of lakes (85 of 129) exhibit at least one major charcoal peak in the interval of 12,800 ± 150 cal BP, and 83% (107 of 129) have at least one charcoal peak in the interval of 12,800 ± 300 cal BP.

Biomass Burning and the Pollen Record. Widespread biomass burning can be expected to have a dramatic effect on vegetation and hence to be recorded in the pollen record. Peros et al.'s (2008) comprehensive analysis of North American pollen records indeed demonstrated that an abrupt, temporary decline in conifer forests (mostly *Picea* sp.) occurred widely across North America during the first 150 y of the YD climate episode. This loss was accompanied by a sudden expansion of *Populus* species (poplar, cottonwood, aspen) and sometimes *Alnus* (birch), which are opportunistic pioneers that often flourish following major forest disruptions such as wildfires. In turn, *Populus* species were replaced by conifers during the remainder of the YD. Thus, a large, pervasive, temporary change in continental vegetation, as reflected in the North American pollen record, is consistent with a major biotic perturbation that would have resulted from widespread biomass burning at the YDB.

Biomass Burning and the Black Mat. Previous investigations have established that the YD onset is marked by the widely distributed deposition of black-mat layers across North America (Firestone at al. 2007; Haynes 2008). The presence of these organic-rich sediments is consistent with an abrupt episode of large-scale biotic degradation that resulted from YD climate change and a major increase in biomass burning (Firestone at al. 2007; Haynes 2008). Haynes (2008) surveyed 97 sites across 23 states in
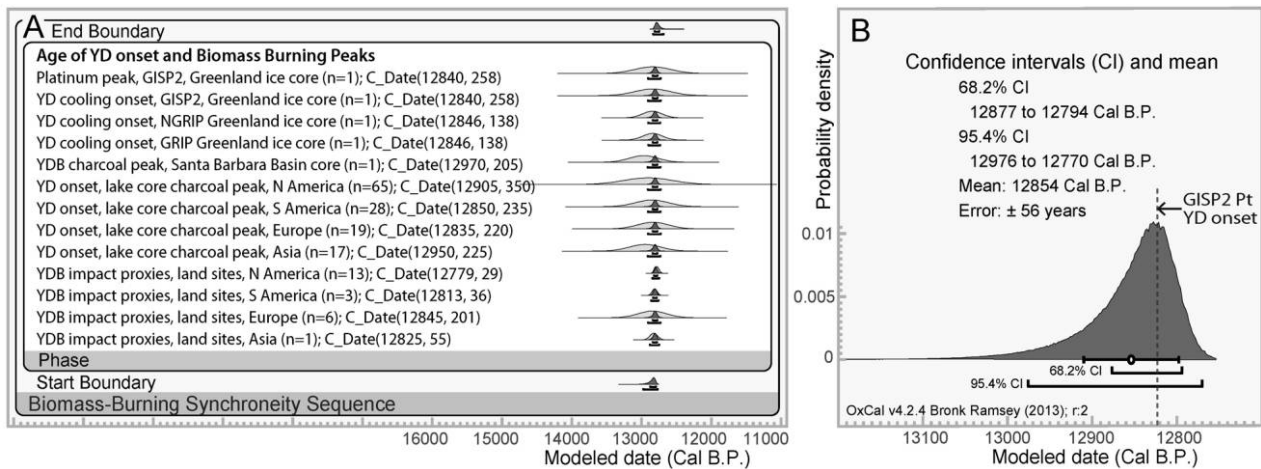
Figure 8. Bayesian synchroneity of climate change, biomass burning, and impact-related proxies at the Younger Dryas (YD) onset. *A*, 13 groups, including ice cores, lake and marine cores, Pt peaks, and sites with YD boundary (YDB) impact-related proxies. Light gray bell curves at right represent unmodeled calibrated age distributions with calculated confidence intervals. Dark gray curves represent modeled isochronous ages for all groups of sites. "C_Date" means that calibrated dates from OxCal or the errors-in-variables (EIV) method, shown in parentheses, were used; n = number of sites per group. Results show that ages for all groups could be synchronous. *B*, Single-model confidence intervals (CIs) for 13 groups of records. Mean age of 157 dates is 12,854 ± 56 cal BP. GISP2 = Greenland Ice Sheet Project 2; NGRIP = North Greenland Ice Core Project; GRIP = Greenland Ice Core Project.

the United States and one province in Canada and found black mats at 72 sites (74%). He also found closely associated remains of extinct megafauna at 73 sites (75%) and the remains of Clovis artifacts at 46 sites (47%). Moreover, Haynes (2008) noted that no in situ megafaunal remains or Clovis artifacts have ever been found above the base of black mat, indicating that it represents both the extinction boundary and the termination of the Clovis culture. This termination is coeval with the decline in other paleohuman populations across the Northern Hemisphere (Anderson et al. 2011).

Not every YDB site exhibits a black mat, but when one is present, biomass-burning proxies and YDB impact proxies reach peak concentrations at the base of or within the black mat. Approximately 40 YDB sites on four continents contain magnetic spherules, meltglass, and one or more biomass-burning proxies. Of the YDB sites investigated for biomass-burning proxies, 83% contain AC/soot, 100% contain BC/soot, 96% contain charcoal, 79% have carbon spherules, and 100% contain nanodiamonds (table 1), thus demonstrating a strong connection between the YDB impact event and synchronous biomass burning. Similarly, Pt has been found at 87% of the sites investigated and precisely correlates with Pt deposition in the Greenland ice sheet. Bayesian-calculated ages for all sites, as shown in figure 8, indicate that the YDB impact event, YD climate change, and widespread biomass burning were synchronous.

Amplitude of Charcoal Peaks at the YD Onset. Bayesian plots of charcoal abundances in lake sequences show broad-based charcoal peaks indicating biomass burning at or close to the YD onset. These results, however, exhibit no high-amplitude, short-duration YDB peaks, such as those as found in the Greenland ice cores. The reasons for this are unclear, but there are several possible explanations. (1) Incompatible radiocarbon calibration curves and/or insufficient chronological resolution for many lake cores might have caused the onset of the YD to have been inaccurately identified with incorrect age-depth models. (2) In addition, the vertical transport of charcoal in sedimentary sequences might cause 12,835-y-old YDB sediments to appear too old or too young, thus blurring the age record (Kennett et al. 2015). (3) By their very nature, lakes are in basins that capture eroded, redeposited sediments across a wide time span (Blong and Gillespie 1978). As a result, the reworking of large amounts of charcoal might continue for decades or even centuries after an individual local wildfire event. (4) Furthermore, even though the YDB impact is thought to have triggered widespread biomass burning, those fires were not ubiquitous, and so not all lake sediments are expected to contain an impact-related charcoal peak. (5) In addition, sharp, brief charcoal YDB-age peaks might be present but muted by the smoothing algorithm used in both the EIV and regression methods. (6) Finally, the extinction of the megafauna
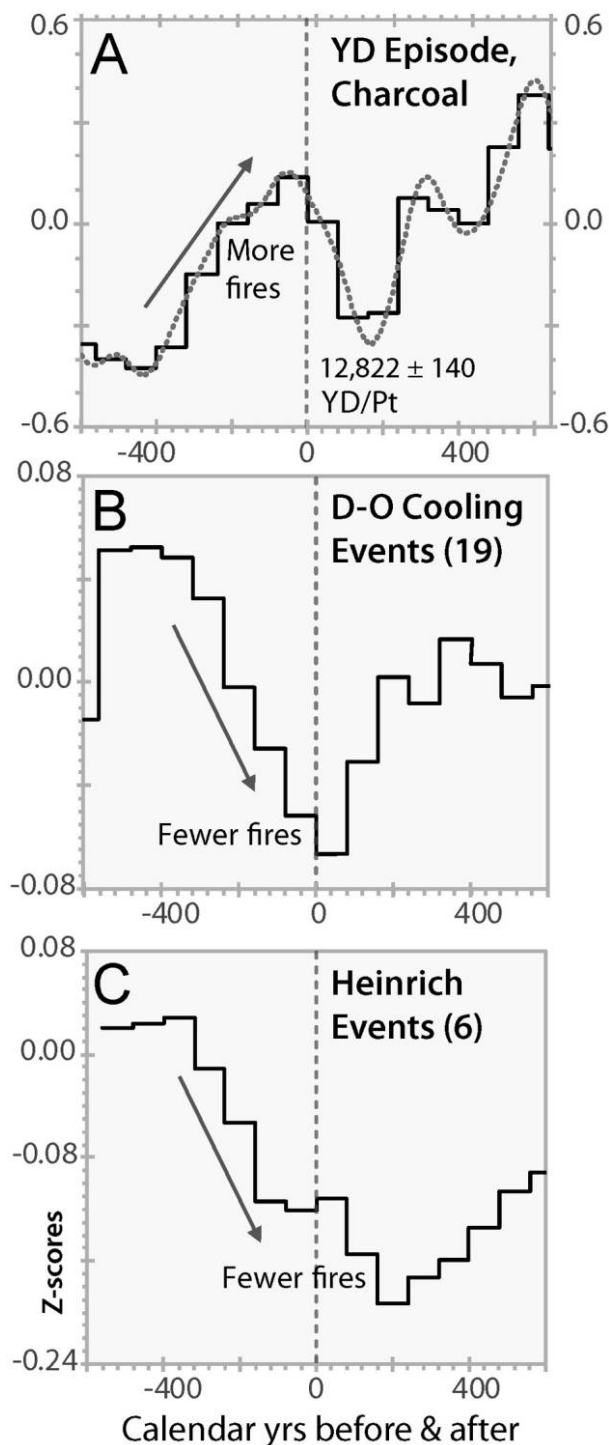
Table 1. Younger Dryas Boundary (YDB) Sites with Proxies

Category, peak evidence	No. of sites examined	Sites with proxies (no.)	Sites with proxies (%)
Biomass-burning evidence:			
AC/soot	24	20	83
BC/soot	19	19	100
Charcoal	26	25	96
Carbon spherules	19	15	79
Black mat	97	72	74
Impact-related proxies:			
Platinum	31	27	87
Magnetic spherules	22	19	86
Nanodiamonds	24	24	100
Extinctions:			
Megafauna	97	73	75
Population decline:			
Clovis culture	97	46	47

Note. Number of sites with biomass-burning proxies, YDB impact-related proxies, megafaunal remains, and Clovis artifacts: sites at which individual proxies have been found, along with percentage of total sites. Source of data for black mats, megafauna, and Clovis artifacts is Haynes (2008). AC = aciniform carbon; BC = black carbon.

would have led to higher fuel loads, resulting in a sustained increase in biomass burning after the YDB event.

The lack of YDB charcoal peaks in some lake-core records indicates either that there were no local fires at that time or that the charcoal has not been preserved. This may result from many factors that affect the preservation of biomass-burning proxies after deposition: (1) erosion of the charcoal-rich layer, (2) desiccation of lakes and ponds, leading to deflation of the YDB layer, (3) dearth of local fuel when the impact occurred, (4) variable accumulation rates of sediment and charcoal, (5) bioturbation that mixed sediment and charcoal of different ages, (6) oxidation and bioassimilation that destroyed

Figure 9. Comparison of Younger Dryas (YD) biomass burning with previous cooling events. *A*, Stair-stepped solid line represents 80-y bins of charcoal *Z*-scores. The gray dashed curve is the Bayesian plot of charcoal *Z*-scores on four continents, the same as shown in figures 3*D* and 4*A*. The dashed vertical line represents 12,822 ± 100 y cal BP, the age of the Greenland Ice Sheet Project 2 Pt spike. *B*, 80-y bins of 19 Dansgaard-Oeschger (D-O) cooling events from Daniau et al. (2010), showing a decreasing trend of biomass burning up to the onset of cooling, opposite to the increasing charcoal trend at the YD onset. *C*, 80-y bins of six previous Heinrich cooling events from Daniau et al. (2010), showing a trend of less or similar biomass burning up to the onset of Heinrich cooling, opposite to the trend of increased biomass burning at the onset of the YD cooling episode, also considered a Heinrich event (Andrews et al. 1995).

charcoal and soot, and (7) very high temperatures near the epicenter that resulted in the formation of ash rather than charcoal and soot.

For future investigations, these limitations could be reduced through higher-resolution sampling, by radiocarbon dating short-lived materials (e.g., seeds), and by using a wider range of biomass-burning proxies (e.g., carbon spherules). In addition, measurement of Pt concentrations could more precisely identify the YD boundary.

Anomalous Wildfires Activity at YD Onset. The question arises whether high peaks in charcoal concentrations were common during non-YD warm-to-cold transitions and whether those at the YD onset are more readily explained by nonimpact processes. Large variations in biomass burning activity are commonly accepted to be climate related, and, if so, similarly high charcoal peaks should appear at other episodes of climate change throughout the record. Daniau et al. (2010) investigated the biomass-burning record during 19 previous Dansgaard-Oeschger rapid-cooling events (fig. 9*C*) and six cold episodes, known as Heinrich events (fig. 9*D*). They found that the typical response to warm-to-cold climate transitions resulted in the lowest wildfire activity in the records, not the highest, as for the YD cooling event. Notably, even though the YD is considered a Heinrich event (designated H0; Andrews et al. 1995), the anomalously high peak in wildfire activity at the YD onset is completely opposite to that of six previous Heinrich events, which showed low levels of biomass burning (Daniau et al. 2010). Daniau et al. (2010) also found that after reaching a low point in biomass burning during previous non-YD cooling events, wildfire activity remained low for approximately a century, whereas, conversely, wildfire activity ramped up for nearly a century after the YD onset. This is a crucial observation: the presence of high peaks in biomass burning at the YD onset is completely contrary to very low levels of biomass burning observed at previous similar climatic transitions, making the YD climate episode highly anomalous and unexplainable by the natural processes that created previous warm-to-cold transitions.

Percentage of YDB Biomass Burned. It has previously been established for the K-Pg impact that the concentrations of AC/soot are directly proportional to the percentage of biomass burned (Wolbach 1990). Thus, it is possible to estimate the burn area of any wildfire episode, including YD-onset biomass burning. We used the amount of measurable AC/soot for seven sites to determine the weighted average YDB AC/soot "footprint" concentration of 0.015 ± 0.005 g (AC/soot)/cm^2 (table A12). While AC/soot concentrations typically have an error of

$\pm 10\%$, samples with especially low concentrations have a slightly higher error because there are fewer aciniform particles to identify and quantify with SEM. After adjustment for these errors, YDB concentrations range up to $0.015 + 0.005$, or 0.020 g (AC/soot)/cm^2.

To calculate the percentage of global biomass burned, we infer that biomass concentrations at the YD onset were roughly equivalent to average contemporary global biomass concentrations of 0.2 g biomass/cm^2 (Seiler and Crutzen 1980). Using the average footprint from above, we can calculate the percentage of global biomass burned:

$$\frac{0.015 \pm 0.005 \,\text{g (AC/soot)/cm}^2}{0.2 \,\text{g biomass/cm}^2} \times 100 = 7.3\% \pm 2.3\%, \tag{1}$$

for a range of ~5 to ~10% biomass burned. Alternately, assuming precivilization biomass concentrations of 0.5 g biomass/cm^2 (Rodin et al. 1975) and using the average footprint above, the percentage biomass burned is

$$\frac{0.015 \pm 0.005 \,\text{g (AC/soot)/cm}^2}{0.5 \,\text{g biomass/cm}^2} \times 100 = 2.9\% \pm 0.9\%, \tag{2}$$

for a range of 2.0%–3.8% biomass burned. Thus, the maximum percentage possible from the available data is 7.3% + 2.3% (eq. [1]), for a total of 9.6% of biomass burned.

Area of Biomass Burned. Still et al. (2003) calculated the area of contemporary global biomass as 106.2×10^6 km^2. This is a conservative value that is less than the area in preindustrial times. We infer here that this area is similar to the amount of biomass at the YD onset, when there was presumably less biomass because of more extensive ice cover and larger nonvegetated areas. As shown in table A12, with the mean value of 7.3% global biomass burned, the estimated global area burned is

$$106.2 \times 10^6 \,\text{km}^2 \times (0.073 \pm 0.023) = (7.7 \pm 2.5) \times 10^6 \,\text{km}^2, \tag{3}$$

for a range of $(5.2–10.2) \times 10^6$ km^2 area burned.

Percentage of Land Area Burned. Global land area is 149×10^6 km^2, and thus, if the YDB impact-related fires are global, the percentage burned is

$$\frac{(7.7 \pm 2.5) \times 10^6 \,\text{km}^2 \,\text{burned}}{149 \times 10^6 \,\text{km}^2} \times 100 = 5.2\% \pm 1.7\%, \tag{4}$$

for a range of 3.5%–6.9% area burned. The Northern Hemisphere land area is 100×10^6 km^2; thus, if the

fires are restricted to this area, the percentage of land burned is

$$\frac{(7.7 \pm 2.5) \times 10^6 \, \text{km}^2 \, \text{burned}}{100 \times 10^6 \, \text{km}^2} \times 100 = 7.7\% \pm 2.5\%, \tag{5}$$

for a range of 5.2%–10.2% of land burned in Northern Hemisphere.

The amount of global biomass burned ranges from 5.0% to 9.6%, (eq. [1]), with a mean value of 7.3%, and this range overlaps the range of 8.5%–9.4% for biomass area burned at the YD onset, as calculated from the Antarctic CO_2 record in part 1 (Wolbach et al. 2018). Hence, the calculated percentage of biomass area burned is similar for two independent biomass-burning proxies, CO_2 and AC/soot.

YDB Burn Rate versus Contemporary Burn Rate. Roy et al. (2008) reported that the global area burned during 2001–2002 was $3.22 \times 10^6 \, \text{km}^2$ per annum. Using the calculated YDB burn area of $(7.7 \pm 2.5) \times 10^6 \, \text{km}^2$ (eq. [5]), as shown in table A12, biomass burning resulting from the YDB impact over a brief interval of time is larger than the annual contemporary fire rate by

$$\frac{(7.7 \pm 2.5) \times 10^6 \, \text{km}^2}{3.22 \times 10^6 \, \text{km}^2} = 2.4 \pm 0.8, \tag{6}$$

for a range of 1.6–3.2 times the contemporary annual fire rate.

Comparison of Area Burned at the YDB with that at the K-Pg Boundary. Wolbach et al. (1990) estimated carbon per square centimeter (not AC/soot) at 11 K-Pg sites and the percentage of AC/soot at each (table A13). Using the same weighted-average method, we estimate the average K-Pg AC/soot in grams per square centimeter so that the data can be directly compared to YDB values. The global K-Pg weighted average footprint is 0.0044 ± 0.0020 g (AC/soot)/cm², which is ~30% of what we observe at the YDB, allowing us to estimate the K-Pg concentration as ranging from 0.0026 to 0.0054 g (AC/soot)/cm². If we use the same contemporary biomass and land mass assumptions used for the YDB calculations, then the percentage of biomass burned was

$$\frac{0.0044 \pm 0.0018 \, \text{g (AC/soot)/cm}^2}{0.2 \, \text{g biomass/cm}^2} \\ \times 100 = 2.2\% \pm 0.9\%, \tag{7}$$

for a range of 1.3%–3.1% biomass burned; the area burned was

$$(106.2 \times 10^6 \, \text{km}^2) \times (0.022 \pm 0.009) \\ = (2.3 \pm 0.9) \times 10^6 \, \text{km}^2, \tag{8}$$

for a range of $(1.4–3.2) \times 10^6 \, \text{km}^2$ area burned; the percentage of land area burned was

$$\frac{(2.3 \pm 0.9) \times 10^6 \, \text{km}^2 \, \text{burned}}{149 \times 10^6 \, \text{km}^2} \times 100 = 1.6\% \pm 0.6\%, \tag{9}$$

for a range of 1.0%–2.2% of land on Earth burned, or

$$\frac{(2.3 \pm 0.9) \times 10^6 \, \text{km}^2 \, \text{burned}}{100 \times 10^6 \, \text{km}^2} \times 100 = 2.3\% \pm 0.9\%, \tag{10}$$

for a range of 1.4%–3.2% of land in Northern Hemisphere burned; and the burn rate was

$$\frac{(2.3 \pm 0.9) \times 10^6 \, \text{km}^2}{3.22 \times 10^6 \, \text{km}^2} = 0.72 \pm 0.29, \tag{11}$$

for a range of 0.43–1.01 times the annual contemporary fire rate within a few weeks.

The amount of biomass that burned during the K-Pg impact is less than one-third that for the YDB. This raises the question of how and why the fires seem to be more pervasive at the YDB than at the K-Pg, an impact event marked by far more massive environmental and biotic changes. There are two possibilities: (1) the calculations are correct, meaning that the YDB experienced more widespread biomass burning, or (2) carbon at the K-Pg boundary most likely has not been preserved as well in the past 66 My as YDB carbon in the past 12,800 y. Even though K-Pg AC/soot was blanketed by a relatively thick layer of sediment within a short time (globally 2–3 cm in a year or less; Wolbach 1990), some portion of it may have been oxygenated by erosion or bioturbation, thus destroying some portion of the AC/soot record.

Is there any evidence that carbon in sediments is lost over time? Herring (1985) noted that charcoal concentrations and fluxes increased in North Pacific Deep Sea Drilling Project (DSDP) cores as samples became younger, signifying increasing fire frequencies over time. However, an alternate interpretation is that the older samples had less carbon because the carbon oxidized in situ, erroneously making older samples appear to have lower fire frequencies. If correct, this is one explanation of why K-Pg carbon values are lower than those for the YDB; the other explanation is that YDB fires were more extensive.

YDB Impact Winter. It is widely accepted that the K-Pg soot concentrations were high enough to block sunlight and produce an impact winter, similar to that predicted to result from nuclear warfare (Crutzen et al. 1984; National Research Council 1985; Mills et al. 2014). If so, the large quantities of AC/soot produced at the onset of the YD almost certainly would have had the same effect.

The atmospheric absorption coefficient of smoke ranges from 10^4 to 6×10^4 cm^2/g (National Research Council 1985), which can be used to calculate the optical-depth range of the AC/soot at the YDB, from

$$1 \times 10^4 \, \text{cm}^2/\text{g} \times (0.015 \pm 0.005) \, \text{g(AC/soot)/cm}^2$$
$$= 150 \pm 50 \, (\text{dimensionless}), \tag{12}$$

to

$$6 \times 10^4 \, \text{cm}^2/\text{g} \times (0.015 \pm 0.005) \, \text{g(AC/soot)/cm}^2$$
$$= 600 \pm 200 \, (\text{dimensionless}). \tag{13}$$

The transmission factor is $e^{-\text{optical depth}}$, so that optical depth $= \infty$ for either case, meaning that visibility was close to zero and little or no light reached Earth's surface while this quantity of soot was in the atmosphere, even during daylight hours.

The contemporary burning rate produces soot with an average atmospheric residence time of 7 d (Horvath 1993). Higher atmospheric soot loading would likely increase the residence time, particularly if the soot entered the stratosphere, and so 7 d should be considered the lower limit. The average time between discovery and control for a modern wildfire was 37 d in 2003 (Westerling et al. 2006), but that time is shorter than that for preindustrial fires because of modern fire suppression efforts and therefore should be considered a lower limit. With this low value, the residence time of sunlight-blocking soot at the YD onset is

$$\sim\!37 \, \text{d (avg. wildfire duration)}$$
$$+ \sim\!7 \, \text{d (AC/soot duration)} = 44 \, \text{d, or } \sim 6 \, \text{wk.} \tag{14}$$

Thus, the negative effects of AC/soot might have persisted for 6 wk or more at the YD onset, blocking all sunlight and causing rapid cooling. Reduced insolation is also expected from the injection of comet dust to the upper atmosphere, as discussed in part 1 (Wolbach et al. 2018). If so, the lack of sunlight would have had widespread and catastrophic biotic effects, including insufficient light for plant photosynthesis

and growth. At the same time, North Atlantic deep-water formation ceased, thus throttling the so-called ocean conveyor and triggering a sustained decrease in near-global temperatures. The changed state of oceanic circulation in the North Atlantic maintained YD cold temperatures for ~1400 y, until the system reverted to its previous state (Broecker 1997; Kennett et al. 2018).

Megafaunal Extinctions. At or near the YD onset in North and South America, at least 85 mammal genera became extinct, including mammoths, mastodons, ground sloths, dire wolves, American horses, and American camels, along with many birds and smaller mammals (Firestone et al. 2007). Haynes (quoted in Hall 1998, p. 6) wrote, "The sudden extinction of the Pleistocene megafauna would be dramatically revealed by explaining that all were gone an instant before the black mat was deposited."

One focus of this article is to explore whether the megafaunal extinctions were synchronous with the YDB impact event, increased biomass burning, YD climate change, and human population declines. See tables A1 and A2 for previously published studies of the following three standout YDB sites.

Blackwater Draw, New Mexico, located near Clovis, is the type site for Paleoindian Clovis projectile points. At this site, a distinctive black-mat layer, dating to the onset of YD climate change, is in direct contact with peaks in magnetic spherules, Pt, Ir, and biomass-burning proxies, including charcoal, glass-like carbon, fullerenes, and PAHs. These proxies are draped conformably over the last known bones of mammoths killed by Clovis hunters, who then abandoned the site for hundreds of years. The evidence from Blackwater Draw suggests that the YDB impact event is coeval with the megafaunal extinctions and a human population decline, along with a peak in biomass burning and with YD climate change.

Murray Springs, Arizona, contains peaks in magnetic spherules, meltglass, nanodiamonds, Pt, and Ir lying immediately beneath a distinctive black mat that dates to the YD onset. Peaks in YDB biomass-burning proxies include charcoal, carbon spherules, glass-like carbon, AC/soot, fullerenes, and PAHs. At this site, several mammoths were killed by Clovis hunters, after which the black mat formed atop the bones and humans abandoned the site for ~1000 y. Thus, the evidence supports the synchroneity of the YDB impact event, increased biomass burning, YD climate change, megafaunal extinctions, and a major human population decline.

Sheriden Cave, Ohio, contains YDB peaks in magnetic spherules, meltglass, nanodiamonds, Pt, and Ir. A charcoal-rich black mat dates to the YD onset and contains peak abundances of charcoal,

AC/soot, carbon spherules, and nanodiamonds that are closely associated with the last known Clovis artifacts in the cave. The black-mat layer is in direct contact with the wildfire-charred bones of two mega-mammals, the flat-headed peccary (*Platygonus compressus*) and the giant beaver (*Castoroidies ohioensis*), that are the last known examples anywhere in the world of those extinct species. The YDB impact event appears coeval with increased biomass burning, YD climate change, the megafaunal extinctions, and a human population decline.

The YD climate change and human overhunting are the two most widely accepted explanations for the megafaunal extinctions, but neither one by itself nor their combination can fully explain the extinctions (Firestone et al. 2007). It is most likely that the megafaunal extinctions resulted from the direct effects of the extraterrestrial impact, combined with indirect effects, including abrupt YD climate change, insufficient food resources, disease, and flooding, all triggered or amplified by the YD event (Firestone et al. 2007). If so, the combination of all these processes would have been more destructive than any single cause alone.

Effect of Biomass Burning on Food Resources. Measurements of AC/soot indicate that within a brief period at the YD onset, up to ~10% of global biomass burned (see eq. [1]). Such a significant loss of potential food supplies would have had a major negative effect, especially on large herbivores that ingested substantial amounts of biomass and secondarily on the predators that hunted them. The production of AC/soot from the biomass burning of trees mostly results from the incineration of leaves, twigs, and smaller branches, but the trunk and roots, which account for ~80% of the mass of a tree, are largely combustion resistant (Perry 1989). Because trees represent ~80% of all modern terrestrial biomass (Pan et al. 2013), ~64% (80% × 80%) is mostly incombustible, meaning that only ~36% of available biomass is the most likely source of YDB AC/soot. If so, the affected percentage of edible biomass burned can be calculated as follows:

$$\frac{9.6\% \text{ of biomass burned}}{36\% \text{ of edible biomass}} = 26.7\% \text{ of edible biomass burned}. \quad (15)$$

The widespread destruction of more than one quarter of edible terrestrial biomass, including grasslands, scrublands, and tundra, would have increased the mortality of large grazing and browsing animals.

AC/Soot and Extinctions. Wolbach (1990) and Kaiho et al. (2016) proposed that the K-Pg impact produced enough AC/soot and dust to block sunlight and trigger major climate change that, in turn, degraded entire ecosystems and contributed to mass extinctions. If so, why were the YDB extinctions less severe than the terrestrial K-Pg extinctions when AC/soot concentrations appear larger? Perhaps the scale of the YDB impacts was smaller than that for the K-Pg, or YDB soot was less concentrated in the stratosphere and thus blocked less solar radiation.

Impact Scenario and Biomass Burning. Studies of the YDB impact, other known impact events, and nuclear detonations allow us to update the YDB impact hypothesis, as follows. Multiple fragments from a large, disintegrating comet collided with Earth ~12,800 y ago (Firestone et al. 2007; Napier 2010). Airburst fireballs and the ejection of molten rocks would have triggered many individual wildfires over wide areas (Firestone et al. 2007; Napier 2010; Bunch et al. 2012; this study), producing one of the largest concentrations of combustion aerosols deposited in the Greenland ice sheet during the past 120,000–368,000 y (Wolbach et al. 2018). In the higher midlatitudes, atmospheric and oceanic temperatures abruptly decreased from warm interglacial to near-glacial conditions within a few months to a year (Manchester and Patterson 2008; Steffensen et al. 2008; Kennett et al. 2018). Atmospheric and cometary dust, along with AC/soot, triggered the rapid onset of impact winter (Kennett et al. 2018; this study). This blocking of sunlight led to a die-off of vegetation (this study). Damage to the ozone layer likely led to an increase in ultraviolet-B radiation reaching Earth's surface, damaging flora and fauna (this article; Pierazzo et al. 2010; Thomas et al. 2015; Wolbach et al. 2018). Increases in nitrogen compounds, sulfates, dust, soot, and other toxic chemicals from the impact and widespread wildfires likely led to an increase in acid rain (Firestone et al. 2007). Increased production of organic matter and burn products from environmental degradation and biomass burning contributed to algal blooms and the subsequent formation of widespread black mats (Firestone at al. 2007; Haynes 2008). The likely reduction in soil-conserving vegetation would have led to higher water runoff, ponding, and increased erosion (Firestone at al. 2007). At or close to the YDB onset, many megafaunal taxa became extinct, and some surviving species experienced population declines and/or evolutionary/population bottlenecks.

Conclusions

In part 1 (Wolbach et al. 2018, this issue), we investigated biomass burning in ice-core records, and here in part 2, we analyze and discuss multiple lake, ma-

rine, and terrestrial records across several continents. We find that the AC/soot and charcoal peaks recorded at the YD onset are consistent with the YDB impact hypothesis. These peaks in biomass-burning proxies are synchronous with peaks in (1) extraterrestrial Pt deposition, (2) high-temperature, impact-related proxies, including Fe-rich spherules, melt-glass, and nanodiamonds, (3) ice-core combustion aerosols, and (4) climate proxies that mark the abrupt onset of YD climate change. This collective evidence makes the YD onset one of the most unusual events in the entire Quaternary, and a cosmic impact is the only known event capable of simultaneously producing all this evidence.

Author Affiliations

1. Department of Chemistry, DePaul University, Chicago, Illinois 60614, USA; 2. Department of Geography, University of Tennessee, Knoxville, Tennessee 37996-0925, USA; 3. Climate Change Institute, University of Maine, Orono, Maine 04469, USA; 4. School of Mathematics and Statistics, University College Dublin, Belfield, Dublin 4, Ireland; 5. Department of Natural Sciences, Elizabeth City State University, Elizabeth City, North Carolina 27909, USA; 6. Geology Program, School of Earth Science and Environmental Sustainability, Northern Arizona University, Flagstaff, Arizona 86011, USA; 7. Instituto de Investigaciones en Ciencias de la Tierra, Universidad Michoacana de San Nicolás de Hidalgo, Morelia, Michoacán, Mexico; 8. Museum of Natural and Cultural History, University of Oregon, Eugene, Oregon 97403, USA; 9. Department of Nuclear Engineering, University of California, Berkeley, California 94720, USA; 10. Restoration Systems, Raleigh, North Carolina 27604, USA; 11. Instituto de Investigaciones Metalúrgicas, departamento de Geología y Mineralogía, Universidad Michoacana de San Nicolás de Hidalgo, CP 58060, Morelia, Michoacán, Mexico; 12. Santa Barbara Museum of Natural History, Santa Barbara, California 93105, USA; 13. Kimstar Research, Fayetteville, North Carolina 28312, USA; 14. Faculty of Science, Charles University, Prague, Czech Republic; Institute of Geology, Czech Academy of Science of the Czech Republic, Prague, Czech Republic; and University of Alaska, 903 Koyukuk Drive, Fairbanks, Alaska 99775, USA; 15. Center of Excellence in Remote Sensing Education and Research, Elizabeth City State University, Elizabeth City, North Carolina 27909, USA; 16. Quaternary Surveys, 26 Thornhill Avenue, Thornhill, Ontario L4J 1J4, Canada; 17. Department of Physics and Astronomy, University of Kansas, Lawrence, Kansas 66045, USA; 18. Department of Geological Sciences, East Carolina University, Greenville, North Carolina 27858, USA; 19. Savannah River Archaeological Research Program, South Carolina Institute of Archaeology and Anthropology, University of South Carolina, New Ellenton, South Carolina 29809, USA; 20. Buckingham Centre for Astrobiology, University of Buckingham, Buckingham MK18 1EG, United Kingdom; 21. Comet Research Group, Dewey, Arizona 86327, USA; 22. Department of Anthropology and Department of Geology, University of Cincinnati, Cincinnati, Ohio 45221, USA; 23. Department of Physics and Astronomy, Washburn University, Topeka, Kansas 66621, USA; 24. Department of Earth Science and Marine Science Institute, University of California, Santa Barbara, California 93106, USA.

REFERENCES CITED

Adatte, T.; Keller, G.; Stüben, D.; Harting, M.; Kramar, U.; Stinnesbeck, W.; Abramovich S.; and Benjamini, C. 2005. Late Maastrichtian and K/T paleoenvironment of the eastern Tethys (Israel): mineralogy, trace and plati-

num group elements, biostratigraphy and faunal turnovers. Bull. Soc. Geol. Fr. 176:37–55.

Anderson, D. G.; Goodyear, A. C.; Kennett, J. P.; and West, A. 2011. Multiple lines of evidence for possible human population decline/settlement reorganization during the early Younger Dryas. Quat. Int. 242:570–583.

Andrews, J. T.; Jennings, A. E.; Kerwin, M.; Kirby, M.; Manley, W.; Miller, G. H.; Bond, G.; and MacLean, B. 1995. A Heinrich-like event, H-0 (DC-0): source(s) for detrital carbonate in the North Atlantic during the Younger Dryas chronozone. Paleoceanography 10(5): 943–952.

Andronikov, A. V., and Andronikova, I. E. 2016. Sediments from around the lower Younger Dryas boundary (SE Arizona, USA): implications from LA-ICP-MS multi-element analysis. Geogr. Ann. Ser. A Phys. Geogr. 98: 221–236. doi:10.1111/geoa.12132.

Andronikov, A. V.; Rudnickaitė, E.; Lauretta, D. S.; Andronikova, I. E.; Kaminskas, D.; Šinkūnas, P.; and Melešytė, M. 2015. Geochemical evidence of the presence of volcanic and meteoritic materials in late Pleistocene lake sediments of Lithuania. Quat. Int. 386:18–29.

Andronikov, A. V.; Subetto, D. A.; Lauretta, D. S.; Andronikova, I. E.; Drosenko, D. A.; Kuznetsov, D. D.; Sapelko, T. V.; and Syrykh, L. S. 2014. In search for fingerprints of an extraterrestrial event: trace element characteristics of sediments from the lake Medvedev-skoye (Karelian Isthmus, Russia). Dokl. Earth Sci. 457: 819–823.

Andronikov, A. V.; van Hoesel, A.; Andronikova, I. E.; and Hoek, W. Z. 2016b. Trace element distribution and implications in sediments across the Allerød–Younger Dryas boundary in the Netherlands and Belgium. Geogr. Ann. Ser. A Phys. Geogr. 98:325–345. doi:10.1111/geoa .12140.

Arakawa, Y.; Li, X.; Ebihara, M.; Meriç, E.; Tansel, I.; Bargu, S.; Koral, H.; and Matsumaru, K. 2003. Element profiles and Ir concentration of Cretaceous-Tertiary (K-T) boundary layers at Medetli, Gölpazari, northwestern Turkey. Geochem. J. 37:681–693.

Arinobu, T.; Ishiwatari, R.; Kaiho, K.; and Lamolda, M. 1999. Spike of pyrosynthetic polycyclic aromatic hydrocarbons associated with an abrupt decrease in δ¹³C of a terrestrial biomarker at the Cretaceous-Tertiary boundary at Caravaca, Spain. Geology 27:723–726.

Belcher, C. M.; Collinson, M. E.; Sweet, A. R.; Hildebrand, A. R.; and Scott, A. C. 2003. Fireball passes and nothing burns—the role of thermal radiation in the Cretaceous-Tertiary event: evidence from the charcoal record of North America. Geology 31:1061–1064.

Blaauw, M., and Christen, J. A. 2011. Flexible palaeo-climate age-depth models using an autoregressive gamma process. Bayesian Anal. 6(3):457–474

Blong, R. J., and Gillespie, R. 1978. Fluvially transported charcoal gives erroneous ¹⁴C ages for recent deposits. Nature 271:739–741.

Broecker, W. S. 1997. Thermohaline circulation, the Achilles heel of our climate system: will man-made CO$_2$ upset the current balance? Science 278(5343):1582–1588.

Bronk Ramsey, C. 1998. Probability and dating. Radiocarbon 40(1):461–474.

———. 2009. Bayesian analysis of radiocarbon dates. Radiocarbon 51(1):337–360.

Buck, C. E.; Christen, J. A.; and James, G. N. 1999. BCal: an on-line Bayesian radiocarbon calibration tool. Internet Archaeol. 7. doi:10.11141/ia.7.1.

Bunch, T. E.; Hermes, R. E.; Moore, A. M. T.; Kennett, D. J.; Weaver, J. C.; Wittke, J. H.; DeCarli, P. S.; et al. 2012. Very high-temperature impact melt products as evidence for cosmic airbursts and impacts 12,900 years ago [author summary]. Proc. Natl. Acad. Sci. USA 109: 11,066–11,067.

Cahill, N.; Kemp, A. C.; Horton, B. P.; and Parnell, A. C. 2015. Modeling sea-level change using errors-in-variables integrated Gaussian processes. Ann. Appl. Stat. 9(2):547–571.

Clark, J. S.; Lynch, J.; Stocks, B. J.; and Goldammer, J. G. 1998. Relationships between charcoal particles in air and sediments in west-central Siberia. Holocene 8:19–29.

Clark, J. S., and Patterson, W. S., III. 1997. Background and local charcoal in sediments: scales of fire evidence in the paleorecord. In Clark, J. S.; Cachier, H.; Goldammer, J. G.; and Stocks, B. J., eds. Sediment records of biomass burning and global change. Berlin, Springer, p. 23–48.

Crutzen, P.; Galbally, I. E.; and Brühl, C. 1984. Atmospheric effects from post-nuclear fires. Clim. Change 6: 323–364.

Daniau, A.-L.; Harrison, S. P.; and Bartlein, P. J. 2010. Fire regimes during the Last Glacial. Quat. Sci. Rev. 29(21–22):2918–2930.

Ebihara, M., and Miura, T. 1996. Chemical characteristics of the Cretaceous-Tertiary boundary layer at Gubbio, Italy. Geochim. Cosmochim. Acta 60(24):5133–5144.

Edwards, K. J.; Whittington, G.; and Tipping, R. 2000. The incidence of microscopic charcoal in late glacial deposits. Palaeogeogr. Palaeoclimatol. Palaeoecol. 164: 247–262.

Firestone, R. B.; West, A.; Kennett, J. P.; Becker, L.; Bunch, T. E.; Revay, Z. S.; Schultz, P. H.; et al. 2007. Evidence for an extraterrestrial impact 12,900 years ago that contributed to the megafaunal extinctions and the Younger Dryas cooling. Proc. Natl. Acad. Sci. USA 104:16,016–16,021.

Florenskiy, K. P. 1965. Preliminary results from the 1961 combined Tunguska Meteorite Expedition. Spectrum Translation and Research, transl. http://abob.libs.uga .edu/bobk/tungmet.html. Originally published in Russian in 1963, Meteoritika 23:3–27.

GCD. 2013. Global charcoal database. Version 2. http:// www.paleofire.org/index.php.

Hall, D. A. 1998. Arizona's famous Clovis sites could be displayed for public. Mammoth Trumpet 13(2):2–6, 20.

Haslett, J., and Parnell, A. 2008. A simple monotone process with application to radiocarbon-dated depth chronologies. J. R. Stat. Soc. C 57(4):399–418.

Haynes, C. V., Jr.. 2008. Younger Dryas "black mats" and the Rancholabrean termination in North America. Proc. Natl. Acad. Sci. USA 105(18):6520–6525.

Herring, J. R. 1985. Charcoal fluxes into sediments of the North Pacific Ocean: the Cenozoic record of burning. *In* Sundquist, E. T., and Broecker, W. S., eds. The carbon cycle and atmospheric CO_2: natural variations Archean to present. Washington, DC, American Geophysical Union, p. 419–442.

Heusser, L. E., and Sirocko, F. 1997. Millennial pulsing of environmental change in southern California from the past 24 k.y.: a record of Indo-Pacific ENSO events? Geology 25:243–246.

Horvath, H. 1993. Atmospheric light absorption—a review. Atmos. Environ. A 27(3):293–317.

Kaiho, K.; Oshima, N.; Adachi, K.; Adachi, Y.; Mizukami, T.; Fujibayashi, M.; and Saito, R. 2016. Global climate change driven by soot at the K-Pg boundary as the cause of the mass extinction. Sci. Rep. 6:28427. doi:10.1038/srep28427.

Kaiser, K.; Hilgers, A.; Schlaak, N.; Mikal, J.; Kühn, P.; Bussemer, S.; and Przegiętka, K. 2009. Palaeopedological marker horizons in northern central Europe: characteristics of Lateglacial Usselo and Finow soils. Boreas 38: 591–609.

Kennett, D. J.; Kennett, J. P.; West, G. J.; Erlandson, J. M.; Johnson, J. R.; Hendy, I. L.; West, A.; Culleton, B. J.; Jones, T. L.; and Stafford, T. W., Jr. 2008. Wildfire and abrupt ecosystem disruption on California's northern Channel Islands at the Ållerød–Younger Dryas boundary (13.0–12.9 ka). Quat. Sci. Rev. 27(27–28):2530–2545.

Kennett, J. P.; Kennett, D. J.; Culleton, B. J.; Aura Tortosa, J. E.; Bischoff, J. L.; Bunch, T. E.; Daniel, I. R., Jr.; et al. 2015. Bayesian chronological analyses consistent with synchronous age of 12,835–12,735 cal BP for Younger Dryas boundary on four continents. Proc. Natl. Acad. Sci. USA 112(32):E4344–4353.

Kennett, J. P.; Kennett, D. J.; LeCompte, M. A.; and West, A. 2018. Potential consequences of the YDB cosmic impact at 12.8 ka. *In* Goodyear, A. C., and Moore, C. R., eds. Early human life on the southeastern coastal plain. Gainesville, University Press of Florida, forthcoming.

Kinzie, C. R.; Que Hee, S. S.; Stich, A.; Tague, K. A.; Mercer, C.; Razink, J. J.; Kennett, D. J.; et al. 2014. Nanodiamond-rich layer across three continents consistent with major cosmic impact at 12,800 cal BP. J. Geol. 122(5):475–506.

Kirova, O. A., and Zaslavskaya, N. I. 1966. Data characterizing the dispersed matter as recovered from the area of fall of the Tunguska meteorite. Meteoritika 27:119–127 (in Russian).

Lynch, J. A.; Clark, J. S.; and Stocks, B. J. 2004. Charcoal production, dispersal, and deposition from the Fort Providence experimental fire: interpreting fire regimes from charcoal records in boreal forests. Can. J. For. Res. 34(8):1642–1656. doi:10.1139/x04-071.

Mahaney, W. C. 2002. Asteroid and cometary impacts. *In* Atlas of sand grain surface textures and applications. Oxford, Oxford University Press. p. 152–160.

Mahaney, W. C.; Somelar, P.; West, A.; Krinsley, D.; Allen, C. C. R.; Pentlavalli, P.; Young, J. M.; et al. 2016*b*. Evidence for cosmic airburst in the Western

Alps archived in Late Glacial paleosols. Quat. Int. 438B:68–80. doi:10.1016/j.quaint.2017.01.043.

Maiorana-Boutilier, A. L.; Mitra, S.; West, A.; Bischoff, J.; Louchouarn, P.; Norwood, M.; Kennett, J.; and Silva, S. 2016. Organic composition of Younger Dryas black mat. Geological Society of America Conference, Southeastern Section, annual meeting, 65th (Columbia, SC), paper 4-1. Geol. Soc. Am. Abstr. Program 48(3).

Manchester, C. W., and Patterson, W. P. 2008. Climate change during the Late Glacial and early Holocene from Lough Monreagh, western Ireland: evidence from carbon and oxygen isotope values of lacustrine marl. EOS: Trans. Am. Geophys. Union 89(53), Fall Meeting suppl., abstract PP13C-1457.

Marlon, J. R.; Bartlein, P. J.; Walsh, M. K.; Harrison, S. P.; Brown, K. J.; Edwards, M. E.; Higuera, P. E.; et al. 2009. Wildfire responses to abrupt climate change in North America. Proc. Natl. Acad. Sci. USA 106:2519–2524.

Mills, M. J.; Toon, O. B.; Lee-Taylor, J.; and Robock, A. 2014. Multidecadal global cooling and unprecedented ozone loss following a regional nuclear conflict. Earth's Future 2:161–176.

Moore, C. R.; West, A.; LeCompte, M. A.; Brooks, M. J.; Daniel, I. R., Jr.; Goodyear, A. C.; Ferguson T. A.; et al. 2017. Widespread platinum anomaly documented at the Younger Dryas onset in North American sedimentary sequences. Sci. Rep. 7:44031. doi:10.1038/srep44031.

Munoz, S. E.; Gajewski, K.; and Peros, M. C. 2010. Synchronous environmental and cultural change in the prehistory of the northeastern United States. Proc. Natl. Acad. Sci. USA 107(51):22,008–22,013.

Napier, W. M. 2010. Palaeolithic extinctions and the Taurid Complex. Mon. Notes R. Astron. Soc. 405:1901–1906.

National Research Council. 1985. The effects on the atmosphere of a major nuclear exchange. Washington, DC, National Academy Press, 93 p.

Pan, Y.; Birdsey, R. A.; Phillips, O. L.; and Jackson, R. B. 2013. The structure, distribution, and biomass of the world's forests. Annu. Rev. Ecol. Evol. Syst. 44:593–622.

Parnell, A. C.; Haslett, J.; Allen, J. R. M.; Buck, C. E.; and Huntley, B. 2008. A flexible approach to assessing synchroneity of past events using Bayesian reconstructions of sedimentation history. Quat. Sci. Rev. 27:19–20:1872–1885.

Peros, M. C.; Gajewski, K.; and Viau, A. E. 2008. Continental-scale tree population response to rapid climate change, competition, and disturbance. Glob. Ecol. Biogeogr. 17:658–669.

Perry, T. O. 1989. Tree roots: facts and fallacies. Arnoldia 49(4):3–29.

Petaev, M. I.; Huang, S.; Jacobsen, S. B.; and Zindler, A. 2013*b*. Large Pt anomaly in the Greenland ice core points to a cataclysm at the onset of Younger Dryas. Proc. Natl. Acad. Sci. USA 110(32):12,917–12,920.

Pierazzo, E.; Garcia, R. R.; Kinnison, D. E.; Marsh, D. R.; Lee-Taylor, J.; and Crutzen, P. J. 2010. Ozone pertur-

bation from medium-size asteroid impacts in the ocean. Earth Planet. Sci. Lett. 299(3–4):263–272.

Power, M. J.; Marlon, J.; Ortiz, N.; Bartlein, P. J.; Harrison, S. P.; Mayle, F. E.; Ballouche, A.; et. al. 2008. Changes in fire regimes since the Last Glacial Maximum: an assessment based on a global synthesis and analysis of charcoal data. Clim. Dyn. 30(7–8):887–907.

Rasmussen, S. O.; Seierstad, I. K.; Andersen, K. K.; Bigler, M.; Dahl-Jensen, D.; and Johnsen, S. J. 2008. Synchronization of the NGRIP, GRIP, and GISP2 ice cores across MIS 2 and palaeoclimatic implications. Quat. Sci. Rev. 27:18–28.

Reimer, P. J.; Bard, E.; Bayliss, A.; Beck, J. W.; Blackwell, P. G.; Bronk Ramsey, C.; Buck, C. E.; et al. 2013. IntCal13 and Marine13 radiocarbon age calibration curves 0–50,000 years cal BP. Radiocarbon 55(4):1869–1887.

Robertson, D. S.; Lewis, W. M.; Sheehan, P. M.; and Toon, O. B. 2013. K-Pg extinction: reevaluation of the heat-fire hypothesis. J. Geophys. Res. Biogeosci. 118(1):329–336.

Rodin, L. E.; Bazilevich, N. I.; and Rozov, N. N. 1975. Productivity of the world's main ecosystems. In Reichle, D. E., ed. Productivity of the world ecosystems: proceedings of a symposium. Washington, DC. National Academy of Sciences, p. 13–26.

Roy, D. P.; Boschetti, L.; Justice, C. O.; and Ju, J. 2008. The collection 5 MODIS burned area product—global evaluation by comparison with the MODIS active fire product. Remote Sens. Environ. 112:3690–3707.

Seierstad, I. K.; Abbott, P. M.; Bigler, M.; Blunier, T.; Bourne, A. J.; Brook, E.; Buchardt, S. L.; et al. 2014. Consistently dated records from the Greenland GRIP, GISP2 and NGRIP ice cores for the past 104 ka reveal regional millennial-scale δ^{18}O gradients with possible Heinrich event imprint. Quat. Sci. Rev. 106:29–46.

Seiler, W., and Crutzen, P. J. 1980. Estimates of gross and net fluxes of carbon between the biosphere and the atmosphere from biomass burning. Clim. Change 2:207–247.

Steffensen, J. P.; Andersen, K. K.; Bigler, M.; Clausen, H. B.; Dahl-Jensen, D.; Fischer, H.; Goto-Azuma, K.; et. al. 2008. High-resolution Greenland ice core data show abrupt climate change happens in few years. Science 321:680–684.

Still, C. J.; Berry, J. A.; Collatz, G. J.; and Defries, R. S. 2003. Global distribution of C_3 and C_4 vegetation:

carbon cycle implications. Glob. Biogeochem. Cycles 17(1):1006. doi:10.1029/2001GB001807.

Svetsov, V. 2008. Thermal radiation and fires after impacts of cosmic objects. In Adushkin, V., and Nemchinov, I., eds. Catastrophic events caused by cosmic objects. Dordrecht, Springer, 207–226. doi:10.1007/978-1-4020-6452-4_6.

Thevenon, F.; Bard, E.; Williamson, D., and Beaufort, L. 2004. A biomass burning record from the west equatorial Pacific over the last 360 ky: methodological, climatic and anthropic implications. Palaeogeogr. Palaeoclimatol. Palaeoecol. 213(1–2):83–99.

Thomas, B. C.; Neale, P. J.; and Snyder, B. R., II. 2015. Solar irradiance changes and photobiological effects at Earth's surface following astrophysical ionizing radiation events. Astrobiology 15(3):207–220. doi:10.1089/ast.2014.1224.

Westerling, A. L.; Hidalgo, H. G.; Cayan, D. R.; and Swetnam, T. W. 2006. Warming and earlier spring increase western U. S. forest wildfire activity. Science 313(5789):940–943. doi:10.1126/science.1128834.

Wolbach, W. S. 1990. Carbon across the Cretaceous-Tertiary boundary. Ph.D. dissertation, University of Chicago.

Wolbach, W. S., and Anders, E. 1989. Elemental carbon in sediments: determination and isotopic analysis in the presence of kerogen. Geochim. Cosmochim. Acta 53:1637–1647.

Wolbach, W. S.; Ballard, J. P.; Mayewski, P. A.; Adedeji, V.; Bunch, T. E.; Firestone, R. B.; French, T. A.; et al. 2018. Extraordinary biomass-burning episode and impact winter triggered by the Younger Dryas cosmic impact ~12,800 years ago. 1. Ice cores and glaciers. J. Geol. 126: XXX–XXX.

Wolbach, W. S.; Gilmour, I.; and Anders, E. 1990. Major wildfires at the Cretaceous-Tertiary boundary. In Sharpton, V. L., and Ward, P., eds. Global catastrophes in Earth history: an interdisciplinary conference on impacts, volcanism, and mass mortality. Geol. Soc. Am. Spec. Pap. 247:391–400.

Wolbach, W. S.; Lewis, R. S.; and Anders, E. 1985. Cretaceous extinctions: evidence for wildfires and search for meteoritic material. Science 230:167–170.

Wolbach, W. S.; Widicus, S. L.; and Kyte, F. T. 2003. A search for soot from global wildfires in central Pacific Cretaceous-Tertiary boundary and other extinction and impact horizon sediments. Astrobiology 3:91–97.